University of Nevada, Reno

Heat and Mass Transfer Studies: Sulfur Diffusion in Polyurethane, Polyphenylquinoxaline as a Heat Exchanger Coating, and Polypropylene Membrane Contactor for Deaeration of Cyanide Solution

A thesis submitted in partial fulfillment of the requirements for the degree of

Master of Science in Chemical Engineering

By:

Marcus Sacchetti

Dr. Alan Fuchs / Thesis Advisor

August, 2015

THE GRADUATE SCHOOL

We recommend that the thesis
prepared under our supervision by

MARCUS SACCHETTI

Entitled

**Heat And Mass Transfer Studies:
Sulfur Diffusion In Polyurethane, Polyphenylquinoxaline As A Heat Exchanger Coating, And Polypropylene Membrane Contactor For Deaeration Of Cyanide Solution**

be accepted in partial fulfillment of the
requirements for the degree of

MASTER OF SCIENCE

Alan Fuchs, Ph.D., Advisor

Vaidyanathan Subramanian, Ph.D., Committee Member

Sage Hiibel, Ph.D., Graduate School Representative

David W. Zeh, Ph.D., Dean, Graduate School

August, 2015

Abstract

This research studied the heat and mass transfer characteristics of several polymers as applied to different applications. Polyurethane was investigated to determine the mass transport rate of sulfur compounds. Polyurethane is commonly used as a potting material for sensitive electronics. Sulfur will readily degrade these components; a projected lifetime can be highly useful to avoid catastrophic failure. Pure sulfur gas exhibited a diffusivity of 4.01×10^{-6} $cm^2 sec^{-1}$. A polyphenylquinoxaline coating was studied for viability as a high temperature heat exchanger coating. The coating had a thermal conductivity of 0.1742 $W(m^2K)^{-1}$ Polypropylene membrane contactors are an efficient method to remove dissolved gases from liquids. The membrane contactor was used to determine suitability in the removal of oxygen from a cyanide solution. Flux of dissolved oxygen across the semi-permeable membrane was observed to be $0.0588 gO_2(m^2 min)^{-1}$.

Acknowledgments

Foremost, I would like to express my sincere gratitude to my advisor Dr. Alan Fuchs, for the support of my Master's research, and his continuous help and guidance throughout my time in the program. Every discussion about a project or class left me with invaluable advice, and direction.

I would also like to thank the other members of my thesis committee: Dr. Ravi Subramanian and Dr. Sage Hiibel. Their insight and experience enriched my work and the final product in a way that I will be eternally grateful for.

My gratitude also goes to the people whom I worked alongside in Dr. Alan Fuchs' laboratory: Wesley Clary, Ying Liu, Jacob Pankey, and Irawan Pramudya. Their contributions go far beyond simply helping with instrumentation or discussion.

I thank my family and friends for their support and willingness to handle the stress I placed upon them. Last but not least Apollo and Gemini were instrumental in persevering through long nights. Never underestimate the sleep schedule of kittens.

Table of Contents

List Of Figures

List of Tables

Chapter I - Introduction

1.1: Background

Polymers are used in a huge variety of applications, from everyday household materials to extensive use in space, such as satellites. The polymers used in your house vary greatly from a plastic bag to shielding on electrical wires. Polymers used in space applications have just as much variation in terms of their applications, from thermal control coatings and adhesives, to potting compounds to protect electrical circuits[1]. Besides the diversity of polymers to many applications, they are also relatively cheap as bulk costs of certain polymers are in the range of $1-2/lb. This low-cost advantage likely prompted significant research in order to replace more expensive materials with cheaper polymeric options.

In this work several different types of polymers are investigated, a polyurethane elastomer, high-temperature aromatic heat exchanger coating, and a polypropylene membrane contactor. While diverse an underlying theme of heat and mass transfer is present. Both the operation of the membrane contactor and diffusion of sulfur compounds through polyurethane follow Fick's law. The heat exchanger coating follows Fourier's law, which is fundamentally similar to Fick's law. The driving force for any mass or heat transfer relies upon

the difference in either concentration or temperature. For the polyurethane elastomer work this is the difference in concentration between the inside of the polyurethane and the experimental chamber containing the sulfur compound. The heat exchanger has a temperature difference between the walls and the fluid moving through, it is important to ensure that the polymeric coating does not inhibit the energy flow drastically. The deareation of the basic cyanide solution can be achieved by creating a large driving force at the interface of the liquid and the membrane. Having a large surface area inside the membrane contactor further assists in the mass transfer out of the liquid stream. While diverse the same principles apply to the characterization of each polymeric material.

1.2: Mass Transport Through Polyurethane Elastomers

Polyurethane can have many physical forms depending upon the branching, crosslinking, and chain length (Figure 1.1).

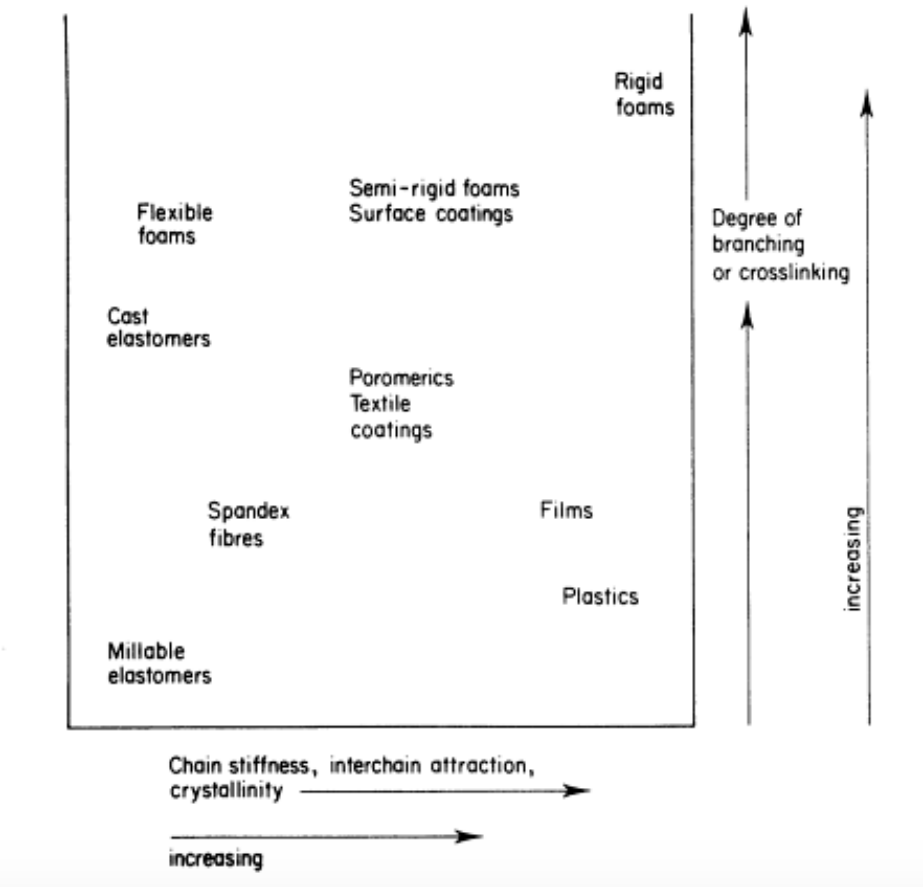

Figure 1.1: Various Structure Property Relationships for Polyurethane.[2]

Polyurethane is highly versatile in the physical forms achievable and therefore in the applications it can be used in as demonstrated in Figure 1.1. The research in the second chapter focuses on a polyurethane elastomer used as a potting material for sensitive electronics. Potting materials are used to protect the electronics from corrosive gases present in the atmosphere, Chapter 2 focuses on sulfur compounds specifically. Polyurethane elastomers consist of three main parts: polyol, diisocyanate, and a chain extender. Changing the ratio

of these three components can produce a jelly to a hard plastic and anything in between[2]. Figure 1.2 shows a basic diagram of what the physical structure of a polyurethane elastomer could be visualized as.

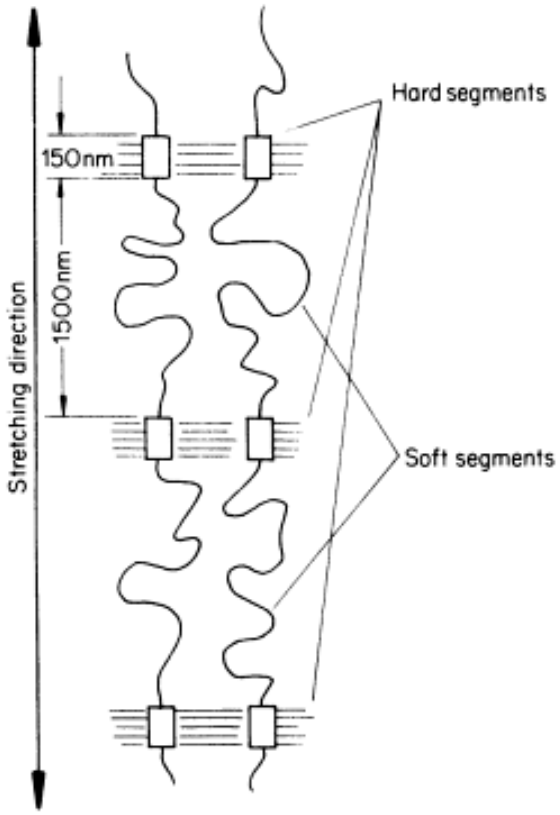

Figure 1.2: Visualization of Flexible and Rigid Segments of a Generic Polyurethane Elastomer. [2]

The ratio of flexible and hard segments in the molecular structure of the polyurethane elastomer determines the final hardness of the polymer. In Chapter 2 the test polyurethane was provided by GE Measurement and Control. To test the validity of the experimental model described for silicone,[3] a commercially available silicone and polyurethane with a Shore hardness of 30 was chosen. A

Shore harness of 30 is slightly softer than a pencil eraser. This polyurethane was chosen as it seemed most similar to the material provided by GE. One thing to keep in mind is that it likely differed considerably on a molecular level but it was close enough to get a reasonable estimate as to whether or not the model would work. The model was also tested with a commercial silicone rubber.

The experiments were performed in the same manner as the ones shown in chapter two. Both sets of experiments below were performed at 110 ^{0}C in a dry environment with sulfur powder. The environmental chamber was vacuum for several minutes to remove as much air as possible and the sulfur powder was allowed to sublime and fill the chamber with sulfur gas. In preliminary testing, a flat sheet was also evaluated. Flat sheet samples after testing are shown in Figure 1.3.

Figure 1.3: Flat sheet silicone sample exposed to a sulfur powder environment at 110 ^{o}C for 24hr, 48hr, 90hr and 120hr.

It is clear from Figure 1.3 that the samples reacted in much the same way as the test tube formed samples used in the other experiments. Figure 1.4 shows the diffusion distance as a function of time for the cylindrical silicone samples.

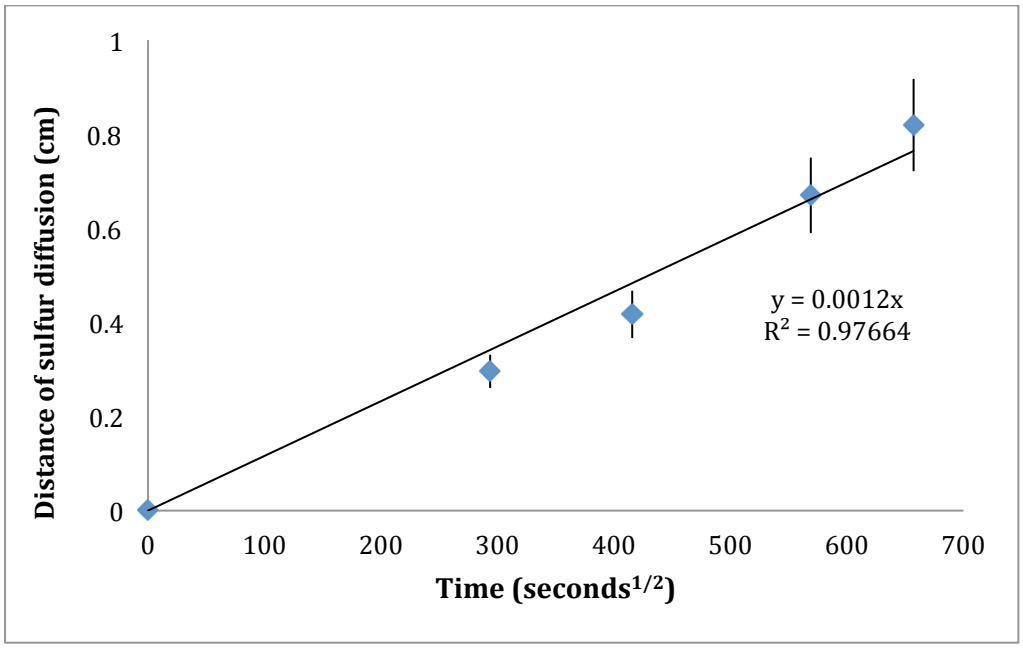

Figure 1.4: Sulfur diffusion distance in a cylindrical silicone sample at 110°C

In Figure 1.4 it is clear that the coefficient of correlation is lower than that observed for the experiments shown in Chapter 2 with the polyurethane provided by GE. With the results from Figures 1.4, 1.5, and 1.6 it is clear that the experimental model is reasonable for use with the industrial polyurethane.

Figure 1.5 shows the diffusion distance as a function of time for the flat sheets of silicone, with the commercial polyurethane

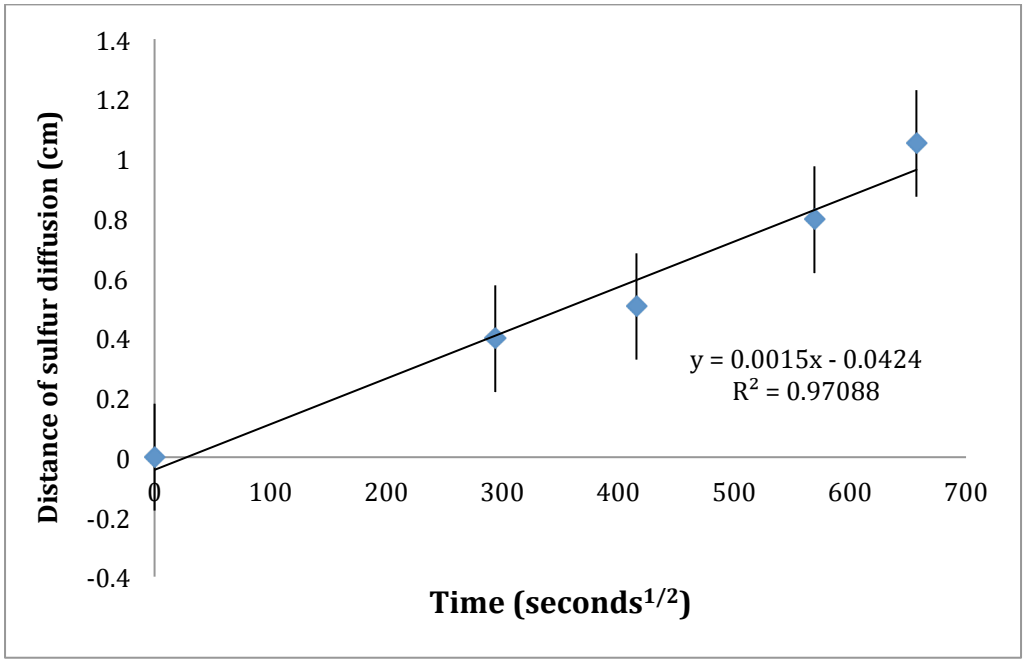

Figure 1.5: Pure Sulfur diffusion through a flat sheet sample of silicone at 110^{o}C

Table 1.1 shows the average value for the permeability with both a flat sheet and cylinder shaped sample of commercially available silicone rubber. The difference in the two values is considerable however given the different shapes as well as any difference that could arise from curing the sample this is not unreasonable. Permeability for the silicone rubber tested in the literature[3] at 120^{o}C is 3.0x10^{-4} (g.cm/sec.cm^{2}.cmHg). Higher temperature and different silicone rubbers reasonably account for this difference.

Table 1.1: Permeability of elemental sulfur in silicone rubber.

Sample	Permeability (g.cm/sec.cm^2.cmHg)
Cylinder	2.0 x10^{-6}
Flat sheet	2.7 x10^{-6}

Table 1.2 shows the experimentally determined permeability, diffusivity, solubility and concentration of pure sulfur in the cylindrical commercial polyurethane samples.

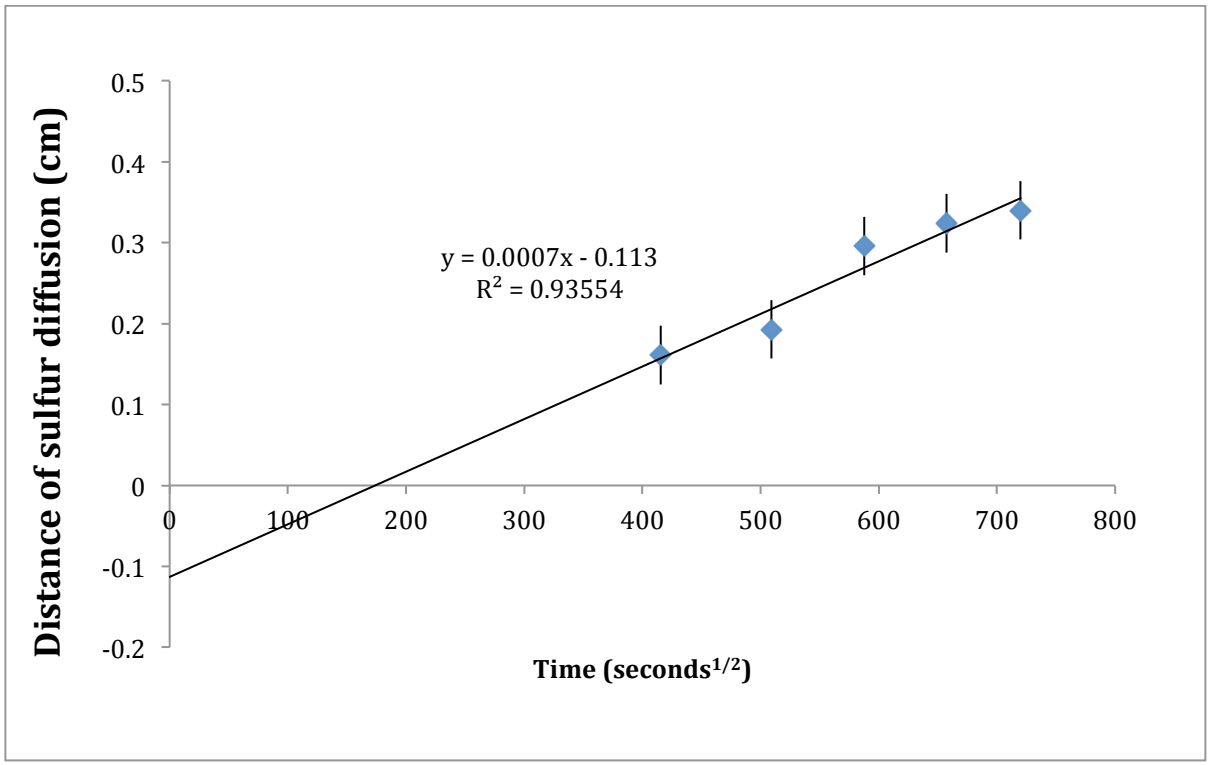

Figure 1.6: Diffusion of sulfur in ClearFlex 30 polyurethane at 120^{o}C

Figure 1.6 shows the diffusion distance of the five samples tested. The distance that sulfur travels through the polyurethane at constant temperature is shown to be linear. In Table 1.2, the permeability, diffusivity, specific solubility of sulfur in polyurethane, concentration of sulfur, length traveled, and times are shown.

Table 1.2: Calculated values for permeability, diffusivity, specific solubility, and concentration.

Sample	P (g-cm/cm^2-sec-cm Hg)	C, (g/cm^3)	Length (cm)	time (h)	S (g/cm^3-cmHg)	D (cm^2/sec)
1	2.016×10^{-7}	1.45×10^{-3}	0.161	48	8.064	2.500×10^{-8}
2	2.080×10^{-7}	1.56×10^{-3}	0.193	72	8.684	2.395×10^{-8}
3	3.685×10^{-7}	1.57×10^{-3}	0.296	96	8.722	4.225×10^{-8}
4	3.510×10^{-7}	1.56×10^{-3}	0.324	120	8.67	4.050×10^{-8}
5	3.174×10^{-7}	1.54×10^{-3}	0.34	144	8.54	3.717×10^{-8}

While the experiments for the commercially available silicone rubber and polyurethane have higher coefficients of correlation the general trend is what was observed with the polyurethane provided by GE and were sufficient for method verification. The disparity in the data set is likely due to the difficulty in removing

the air bubbles when curing the samples in the laboratory. Samples provided by GE were produced in a facility with the necessary equipment to remove any air present in the sample. Even considering the difficulty in manufacturing samples in the laboratory, the results were still reasonable. Since the industrial polyurethane elastomer had much lower disparity, the results appear to be valid. As discussed previously, great differences are possible in any elastomer even if similar properties are present, and the unfortunate fact is that any sample of polyurethane will potentially react differently to the sulfur environment. In order to lower the solubility, permeability, and diffusivity of sulfur to the polyurethane or any other potting material, it is necessary to utilize a much denser material such as an epoxy. There is considerable research potential in the development of new materials for the protection of electronics from corrosion.

1.3: Characterization of Polyphenylquinoxaline as a Heat Exchanger Coating

Polyphenylquinoxaline (PPQx) is a polymer with excellent high-temperature stability. PPQx synthesized in the method as described in Chapter 3 is a film-former, giving it the ability to form a coating with ease. When considering a polymer for a heat exchanger coating the polymer must be able to withstand repeated heating and cooling as well as exposure to high temperatures for extended periods of time. PPQx was able to retain its adhesion to the stainless steel surface even after 50 cycles of heating and cooling to 200^{o}C. Due

to repeated heating and cooling as a result of maintenance or shutdown of the heat exchanger over the life of the coating it was important to ensure that the polymer would retain adhesive strength. Even after the coating must be reapplied a small amount might still be present that would then continue to be exposed to the harsh conditions.

To observe wear on the coating a dye was added to the solution to color the coating. The basis being that a layer with dye would be applied below a layer without the dye so as to observe when the coating was getting close to needing to be replaced. The dye chosen was Amaplase Red BSR, a high-temperature dye soluble in organic compounds. Figure 1.7 shows three different concentrations of the dye. The concentrations are reported as weight percent of PPQx.

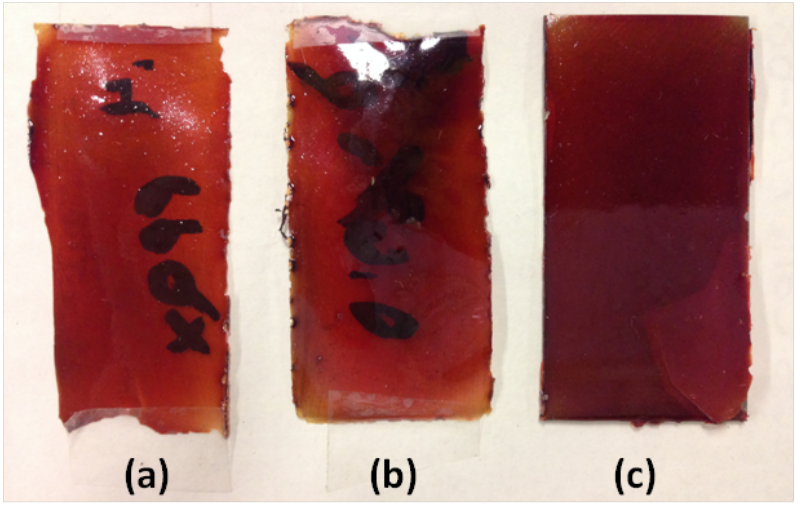

Figure 1.7: PPQx coating with dye, (a) 0.4%, (b) 0.6% and (c) 0.8%.

In Figure 1.7 the coating is just laying on the counter, no longer attached to the stainless steel coupon it was applied to. While the coloring of the coating is excellent and clear, the adhesion of the film was negatively impacted. The film fell off of the stainless steel when it was finished drying and exhibited no adhesive properties as were observed without the dye. After being exposed to heat for extended periods of time, the coating appeared to darken due to oxidation, this could have also made the dye difficult to see and is another possible drawback to using a dye as a wear indicator.

Testing of the thermal properties was done with an Omega Engineering heat flux sensor. The thermal conductivity test set up is shown in Figure 1.8. The heat flux sensor (3) is placed between the heating foil (4) and the coated stainless steel coupon (1). Another thermocouple (2), is then placed on top of the polymer surface of the stainless steel coupon. Figure 1.9 shows the data readout for the test station when it is in operation.

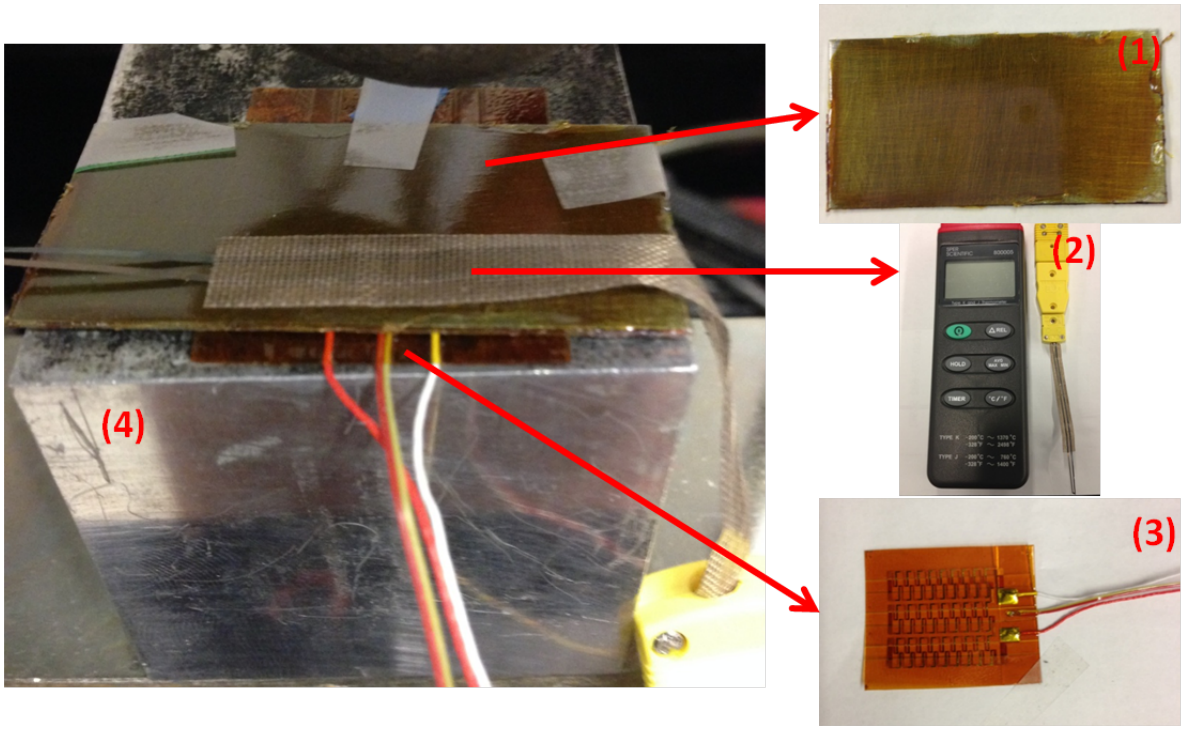

Figure 1.8: Thermal conductivity test apparatus.

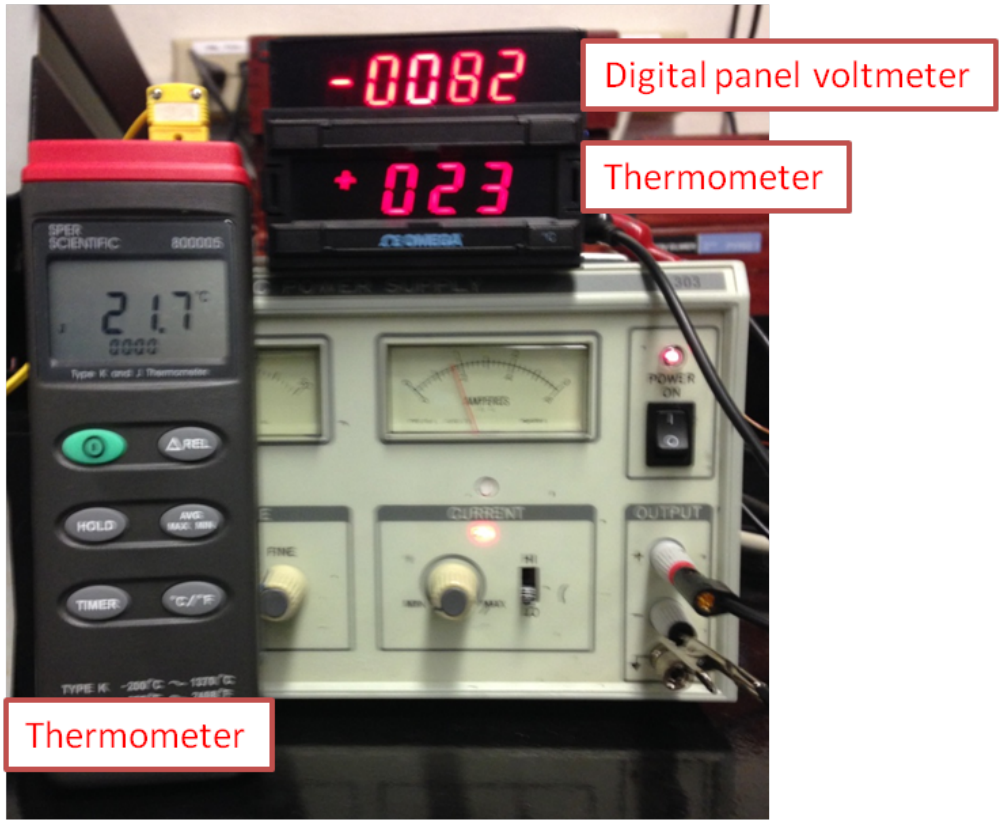

Figure 1.9: Data collection system for thermal conductivity.

When heating is applied to the thermal conductivity experimental apparatus the temperature difference (ΔT) between the two surfaces of the stainless steel coupon is recorded using thermocouples. The heat flux sensor measures the thermal energy transfer per unit time/ unit area. Heat flux is directly proportional to the temperature difference across the thermal resistance barrier. The digital voltmeter then records the voltage output from the heat flux sensor, in microvolts, which are then converted to w/m^2.

Thermal conductivity is calculated using Equation 1:

$$Q = \frac{k}{\Delta L} \times \Delta T \quad (1.1)$$

In Equation 1.1, Heat flux is Q (w/m^2), ΔL is the thickness of the sample (m), ΔT is the temperature difference between the two layers, and k is the thermal conductivity in (w/m^{2}K). Detailed results and description of this experiment as well as the other characterization techniques employed are in Chapter 3.

1.4: Membrane Filtration

To explore another application of polymers it is necessary to move into membrane filtration. Membrane filtration can be applied to liquid/liquid filtration such as dialysis, or liquid/gas filtration such as carbon dioxide capture in flue gas or deaeration as is discussed in Chapter 4. Focusing on what is discussed in Chapter 4 where gases are removed from a liquid stream, it is necessary to investigate why a difficult to manufacture membrane might be desirable. In order to remove dissolved gases from solution several different methods can be employed; and of these some are more applicable to either an industrial or laboratory scale setting. In a lab scale setting a solution can be degassed by a

chemical addition, a freeze/thaw/freeze process, bubbling of a purge gas, or simply holding the solution under a vacuum for an extended period. While none of these methods are quick or efficient, at a laboratory scale where degassing is not often required this can be sufficient. On an industrial scale a vacuum tower might be used, however if space is in short supply this is not an efficient option because of the large footprint. In addition to the large size a vacuum tower could require workers to ascend high places for maintenance, which may be a safety concern. Membrane contactors can solve both of these problems because of their extremely high surface area to volume ratios. A typical membrane contactor for deaeration can have a surface area to volume ratio of $2000m^2$ per m^3.[4] Membrane contactors can be operated in several different ways depending on the application, with a vacuum applied to one side of the membrane, or a purge gas, or a combination of both purge gas and vacuum. When using a purge gas it is generally operated in a counter current mode to take full advantage of the driving force across the membrane. Membrane contactors are versatile in their construction and are available in sizes ranging from small lab-scale contactors capable of processing several milliliters per minute, to large industrial-size contactors capable of processing over one cubic meter per minute. The large-scale contactors can be combined in parallel to increase capacity in order to handle large process volumes[4]. Another advantage, of membrane contactors, in addition to a large surface area to volume ratio, is that they scale linearly. This is especially effective when taking a pilot-scale system up to full design flow. This gives a customer the ability to easily visualize the pilot scale system operating in

their process as a full-size unit operation, removing any question of the potential effectiveness of the end product. The linearity of scale for membrane contactors is due to their well-known surface area per unit. When resizing or expanding a system this becomes a critical feature because more units can be added or units can be removed easily due to modular design associated with a membrane system. This is much simpler and cost effective than attempting to resize a vacuum tower for deaeration in order to achieve a higher process flow. In some cases installation can be difficult for a particular application due to specific space requirements of the deaeration or gas absorbing method in use. Membrane contactors do not have any specific orientation requirements and their footprint is quite small in comparison to their surface area to volume ratio. These factors all combine to make membrane contactors highly desirable as an industrial unit operation.

The membrane fibers are fabricated out of polypropylene, a hydrophobic polymer, and the pores to facilitate gas transfer in a liquid to gas membrane contactor are on average 0.05 microns[4]. The hydrophobic membrane allows both phases to be in contact with one another yet does not allow them to mix. The membrane fibers do not enhance the transport of gases out of the liquid phase but give a way to have a small apparatus with a very high surface area to volume ratio. This large amount of surface area lowers the amount of diffusion that must occur in the liquid phase to move the gas out of or into the liquid. The benefits of this can be clearly seen when considering that the diffusivity of a gas

in air is in general approximately 10,000 times faster than that of the gas in water[5].

Despite all of the advantages of hollow-fiber membrane contactors, there are significant disadvantages that must be considered. The disadvantages are, the possibility of fiber damage, breakthrough, wetting, and cost. Hollow-fiber membrane contactors are generally expensive due to difficult fabrication; even a small module capable of processing only one gallon per minute costs around $1500. This is surprising because the material costs are quite low as most polymers only cost around $1-2/lb. Polypropylene in particular hovers around 90 cents per pound based on Alibaba bulk pricing. The small module mentioned previously has a weight of around 2 pounds, demonstrating the overwhelming majority of cost is due to the fabrication of the membrane contactor. Fiber damage can occur easily if any solids are present in the liquid stream due to the small pore size and operation with liquid on one side of the fiber. If the solids can pass through the membrane pores it is likely that they would become stuck in the module because of the low gas flow rates in use. Wetting is an issue and can be related to breakthrough but at a lesser extent. Wetting and its effects upon efficiency will be discussed in depth later on in Chapter 4. A visualization of wetting is shown in Figure 1.10 in relation to mass transfer.

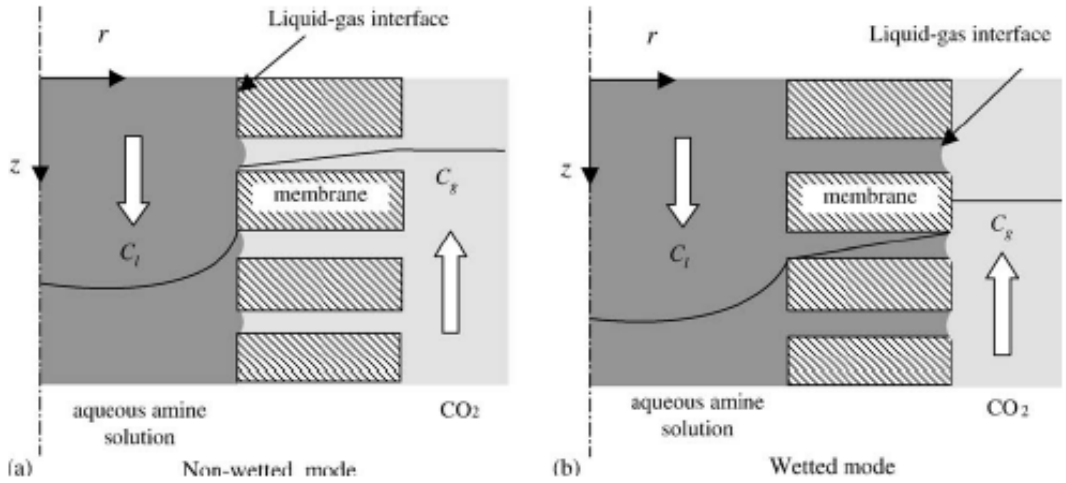

Figure 1.10: Shaded pores represent membrane wetting, with clear pores representing non-wetted conditions.[6]

It is clear that in the case of membrane wetting, mass transfer of gas from the liquid phase to the gas phase is highly inhibited. This would be similar to attempting to reaerate a bottle of water with a long neck with the cap off. The liquid in the neck would reaerate rather quickly however the bulk fluid would take significantly longer to equilibrate. Membrane contactors operate on the opposite principle, the jug has a small surface area to volume ratio, and as a result takes a long time to reach equilibrium, whereas the membrane contactor can maximize the surface area to volume ratio and equilibrate quickly.

To understand the operation of a membrane contactor Fick's law must be employed, while Henry's law (Equation 2).

$$H_e = \frac{p}{c} \qquad [2]$$

provides the first principle foundation to determine the driving force for a membrane contactor. As a result of the lower solubility of a gas when the partial pressure of that gas, above a fluid is reduced there is mass transfer between the two phases. The rate of mass transfer can be calculated by employing Fick's first law. Fick's first law is shown in Equation 3.

$$J = k_l \frac{dx}{dc} \qquad [3]$$

Where J is equal to the flux across a specified area per unit time with units of $kg*m^{-2}*s^{-1}$, k_l is the mass transfer coefficient for the mass transport across the boundary and has units of s^{-1}, dx/dc is equal to the concentration gradient driving the mass transport. Fick's law is one of the most common methods to model diffusion in a system. Models of hollow-fiber membrane contactors can be simplified in relation to that of a flat sheet because only diffusion in one direction need be considered. This is a benefit of the cylindrical design. Diffusion along the length of the contactor can generally be disregarded, as advection is the primary mode of transport, similar to a river. Considering this, as well as the major direction of diffusion is from the center of the flow in the fiber to the outer edge, the assumption of one-directional mass transfer is not unreasonable. Other methods to model diffusion in a system such as a porous media, a membrane contactor system can be to consider the membrane to be a porous media, in this case the dusty gas model, advective-diffusive model, and the Schofield model

can be used.[7] The dusty gas, advective-diffusive, and Schofield models are constructed with the porous media effect in mind. Fick's law does not and is better suited to diffusion in open spaces. In the case of the porous media models they include a parameter to account for the effect of Knudsen diffusion; the interaction of the gas molecules with the porous media.[8]

The aforementioned models are generally focused on gas/gas or liquid/liquid diffusion whereas in this case the interest lies in a liquid being stripped of dissolved gases. Much of the literature is focused on the absorption of carbon dioxide into amine solutions. The interest in this application of membrane contactors is obvious due to the high dependence on fossil fuels and goal of reducing carbon dioxide emissions into the atmosphere. For this application the contactors remove carbon dioxide from the flue gas emission of the coal-fired power plant. If no reactions are being considered then the modeling of carbon dioxide capture is very similar to that of deaeration. While the physical properties of the diffusion and subsequent capture of carbon dioxide differ from the removal of dissolved oxygen from water, the same fundamental driving force applies to the process. So long as no reaction term is being considered[9], in Fick's Law, with the carbon dioxide capture the model formulation will be the same as with the liquid-oxygen system. This similarity is due to the fact that Henry's law still governs the mass transfer and Fick's law can help elucidate some information about that transfer.

Several papers give an in depth analysis of Fick's law as well as couple experiments with the modeling to validate the results.[9,10] Dindore et. al; explore

membrane contactors due to their use as a model contactor that has clearly defined parameters such as interfacial contact area. Another key parameter is the flow regime, in the case of a hollow-fiber membrane contactor this is usually laminar in nature. Considering the laminar flow regime a mass transfer model can be developed based upon first principles. For mass transfer across a contact area the applicable first principle is Fick's law. Dindore et. al; use the analysis that since the Reynolds number for the liquid stream is less than 2100, the flow regime is laminar. This allows them to determine the mass transfer coefficient for Fick's first law, shown in Equation 1, by using a mass transfer analogy of Leveque's heat transfer solution. This incorporates several parameters such as the length of the membrane, diffusivity of the solute to move out of the solvent, and the velocity of the liquid. The models proposed by both Malek et, al and Dindore, et, al; do not take into account for any changes in the gas flow rate, liquid stream pressure, or purge gas pressure. All of the aforementioned parameters would be expected to have significant effect upon the flux of a dissolved gas across the membrane boundary. The data presented in Chapter 4 demonstrates that these parameters do not have a significant effect, although purge gas pressure would likely be the first to have an effect when extended outside of the tested regime in Chapter 4. One can expect the pressure of the purge gas to inhibit gas transfer from the liquid due not to the concentration gradient but the excess pressure on the lumen-side of the membrane contactor. The quantifiable economic advantage of a membrane contactor system for a Merrill-Crowe process and give a design review of

implementation of the system for Merrill-Crowe, both as a new system or replacement system is described in Chapter 5 and Appendix A respectively.

1.5 References:

[1]Krishnamurthy, V. N. Polymers in Space Environments *Polymers and Other Advanced Materials* 221-226, 1995

[2]Hepburn, C. Polyurethane Elastomers *Elsevier Applied Science* 2nd ed. 2012

[3]G. Digiacomo, and E. Spaulding, A Method for Determining the Permeability and Solubility of Sulfur in Poly(dimethylsiloxane) (RTV), *Journal of Applied Polymer Science*, (1979), 23, 261-274.

[4]Wiesler F., Membrane Contactors: An Introduction to the Technology. Ultrapure Water *1996.*

[5]Haynes, William M.., and David R. Lide. *CRC Handbook of Chemistry and Physics a Ready-reference Book of Chemical and Physical Data: 2011-2012.* Boca Raton (Fla.): CRC, 2011. Print.

[6]Wang, R. Zhang, H.Y. Feron, P.H.M. Liang, D.T. *Influence of Membrane Wetting on CO_2 capture in microporous hollow fiber membrane contactors* Separation and Purification Technology 46 33-40, 2005.

[7]Rao, Guiying, Sage R. Hiibel, Andrea Achilli, and Amy E. Childress. *Factors contributing to Flux Improvement in Vacuum-enhanced Direct Contact Membrane Distillation.* Desalination: 197-205. 2015.

[8] Webb, Stephen W., Karsten Pruess. *The Use of Fick's Law for Modeling Trace Gas Diffusion in Porous Media*. Transport in Porous Media: 327-341, 2003.

[9]Dindore, V.Y. Et. al, *Hollow fiber membrane contactor as a gas-liquid model contactor,* Chemical Engineering Science, 467-479, 2005.

[10]Malek, A. Li, K. Teo, W.K. *Modeling of Microporous Hollow Fiber Membrane Modules Operated under Partially Wetted Conditions,* Ind. Eng. Chem. Res. 784-793, 1997.

[11] Marsden, John, The Chemistry of Gold Extraction, Littleton, CO: Society for Mining, Metallurgy, and Exploration, 2006. Print.

Chapter II: Sulfur Mass-Transport In Polyurethane

2.1 Abstract:

This research studied in detail the mass transport of sulfur through polyurethane; we believe this information can be used to successfully predict a lifetime of electronics exposed to harsh sulfur environments. Using the mass transport data given for the different sulfur environments tested, a worst-case scenario can be predicted. In sensitive applications the electronics can be replaced before they would fail due to corrosion.

- Hydrogen sulfide diffuses in polyurethane and reacts with silver particles rapidly (4.74 $x10^{-6}$ cm^2/sec) with sulfur vapor (4.01 $x10^{-6}$ cm^2/sec) and sulfur dioxide being the least aggressive (5.13 $x10^{-7}$ cm^2/sec)
- Humidity also greatly reduced the diffusion rates for sulfur vapor - 58.1%, sulfur dioxide - 38.9%, and hydrogen sulfide - 21.1%, because of competition for active sites.

2.2 Background:

The rate of mass transport of sulfur through polyurethane can be used to predict the lifetime of electronics exposed to harsh sulfur environments. Using the mass transport data given for different sulfur environments, a worst-case

scenario can be predicted. In sensitive applications, this allows for the electronics to be replaced before they would fail due to corrosion.

The corrosion of silver components in electronics, by sulfur gas, has been studied for several decades.[1] One way of protecting the silver components has been to place a polymeric material on the surface. This material, unfortunately, is still permeable to sulfur gas. As a result of the low vapor pressure of sulfur at atmospheric conditions, testing the transport properties by traditional methods is difficult. Different methods have been developed to calculate the transport parameters, such as by using a radioactive sulfur isotope such as S^{35} . While effective, these methods are extremely complex[3,4]. A much simpler method, without the need for expensive materials and equipment has been developed for use with polydimethylsiloxane[2]. This method takes advantage of the corrosive properties of the sulfur gas and uses silver powder as an indicator in the elastomer. Reaction scheme 1 shows the reaction for elemental sulfur and silver.

$$2Ag(s) + S(g) \text{ è } Ag_2S(s)$$

Reaction Scheme 1

Reaction Schemes 2, and 3 show the mechanism for sulfur dioxide to react with the silver powder present in the polyurethane and hydrogen sulfide, respectively.

$$2SO_2 + 2H_2O + O_2 \rightarrow 2H_2SO_4$$

$$2Ag + 2H_2SO_4 \rightarrow Ag_2SO_4 + 2H_2O + SO_2$$

Reaction Scheme 2

Even though the corrosion reaction for sulfur dioxide has two steps in comparison to the single step reactions for hydrogen sulfide and sulfur powder, this does not appreciably impact the transport rates observed. This is due to the fact that the timescales of the reactions are much shorter than those of the mass transport.

$$2Ag(s) + H_2S(g) \rightarrow Ag_2S(s) + H_2(g)$$

Reaction Scheme 3

The reactions shown above are what make the simple indicator type method possible. The experimental section discusses how applied this method.

We used the method employed by Digiacomo[2] to characterize sulfur diffusion in a polyurethane. The parameters we studied were permeability, diffusivity, and solubility. We conducted experiments in a variety of conditions to observe the effect of humidity upon the parameters as well as different sulfur compounds. Significant differences were observed between the sulfur compounds and influence of humidity.

Permeability and Diffusivity Calculations:

In order to calculate the mass transport parameters the following equations developed by Digiacomo[2] were employed.

$$\frac{\rho_R L^2}{2\Upsilon t} = \overline{P_0} P_0 \qquad 1$$

Equation 1 was used to calculate the permeability of sulfur in polyurethane, where ρ_R is the density of reacted sulfur, g/cm^3 of polymer; L is the distance traveled by the sulfur through the sample, cm; Υ is the ratio of sulfur ingress area to the sample container cross-section, t is the time the sample was exposed to the sulfur environment, sec$^{1/2}$; $\bar{P}_0$ is the permeability, g.cm/sec.cm^2.cmHg; and P_0 is the vapor pressure of sulfur, cm-Hg.

$$\tau = \frac{l^2}{6D} \qquad 2$$

Equation 2 was used to calculate the diffusivity of sulfur in polyurethane, where t is the time the sample was exposed to the sulfur environment, sec; l is the distance traveled by the sulfur through the sample, cm; and D is the diffusivity of sulfur in polyurethane, cm^2/sec.

$$\bar{S} = \frac{\bar{P}}{D} \qquad 3$$

Equation 3 is a ratio of the previously calculated permeability and diffusivity, where $\bar{S}$ is the specific solubility of sulfur in the sample, g/cm^3-cmHg; $\bar{P}$ is the permeability, g.cm/sec.cm^2.cmHg; and D is the diffusivity of sulfur in the sample, cm^2/sec.

2.3 Experimental:

The polyurethane prepared in glass test tubes, which are broken off before testing. The sample is then wrapped tightly in aluminum foil. Since the samples are wrapped with aluminum foil only one end of the sample cross section is exposed to the environment of the temperature-controlled oven. The samples of polyurethane had been doped with 1% by mass silver powder as a diffusion front indicator. The silver powder was purchased from Sigma-Aldrich and had an average particle size of 5-8 microns, with a purity of ≥ 99.9%. Figure 2.1 shows the expected response of the sample to the sulfur environment.

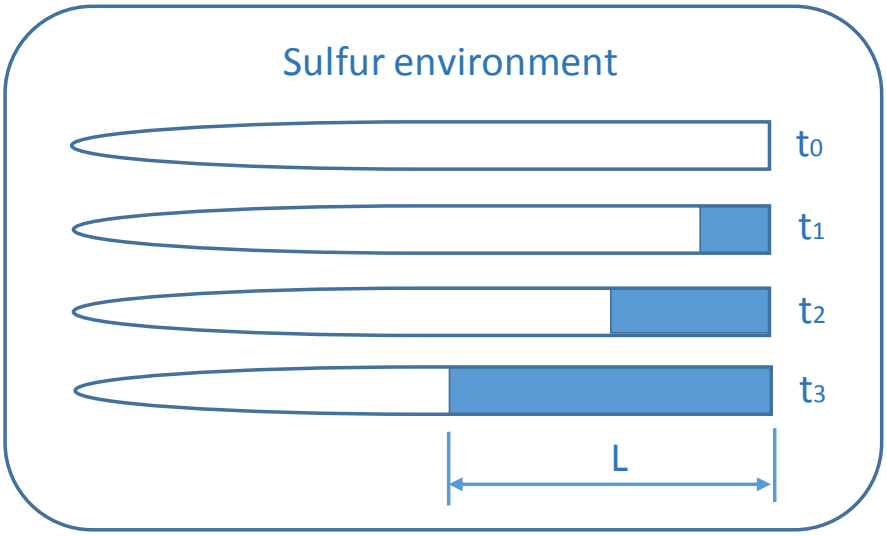

Figure 2.1: Sulfur diffusion in silver powder doped polyurethane.

Silver turns black when corroded by sulfur, which allowed the diffusion front to be easily traced. Polyurethane was exposed to three different sulfur environments, pure sulfur powder, sulfur dioxide gas, and hydrogen sulfide gas. Sulfur powder was purchased from Sigma-Aldrich and had a purity of 99.8%. Sulfur dioxide and hydrogen sulfide were purchased from Airgas and had purities of 99.98% and 99.5% respectively. For each experiment the environment of the test chamber was purged of all atmosphere with a vacuum pump. When testing the two sulfur gas compounds the chamber was vacuumed and backfilled 3 times to ensure a complete environment of either sulfur dioxide or hydrogen sulfide. Table 2.1 outlines the different test methods employed to simulate different sulfur environments. Each set of samples was left in the sulfur environment for differing amounts of time depending upon the transport rate of sulfur through the material. The timeframes are denoted in the results for each experiment.

Table 2.1: Testing conditions for different elastomer experiments.

Conditions	110°C 2.5g sulfur powder	110°C 2.5g sulfur powder (humid conditions)	110°C 1atm pressure sulfur dioxide gas & hydrogen sulfide (dry and humid conditions)

2.4 Results and Discussion:

Upon exposure to the sulfur environment, the samples appear as shown in Figure 2.2.

Figure 2.2: Polyurethane samples after exposure to sulfur

The time of exposure for each sample from left to right is 12 hours, 48 hours and the two right most samples were exposed for 120 hours.

2.4.1 Polyurethane and Sulfur Powder Experiments:

In Table 2.2 the permeability, diffusivity, specific solubility of sulfur in polyurethane, concentration of sulfur, length traveled, and time are shown. Table 2.3 shows the same parameters as Table 2.2 except the data was obtained for samples in the humid environment.

.

Table 2.2: Calculated values for permeability, diffusivity, specific solubility, and concentration at 110C in a dry atmosphere.

Sample	P (g-cm/cm^2-sec-cm Hg)	C, (g/cm^3)	Length (cm)	time (h)	S (g/cm^3-cmHg)	D (cm^2/sec)
1	1.02×10^{-6}	1.54×10^{-3}	0.187	13.6	0.238	4.27×10^{-6}
2	7.76×10^{-7}	1.52×10^{-3}	0.219	24.1	0.234	3.32×10^{-6}
3	9.55×10^{-7}	1.57×10^{-3}	0.298	37.6	0.243	3.94×10^{-6}
4	1.04×10^{-6}	1.52×10^{-3}	0.357	48	0.235	4.43×10^{-6}
5	9.60×10^{-7}	1.51×10^{-3}	0.389	61.3	0.233	4.11×10^{-6}

Table 2.3: Calculated values for permeability, diffusivity, specific solubility and concentration at 110C in a sulfur environment saturated with water vapor.

Sample	P (g-cm/cm^2-sec-cm Hg)	C, (g/cm^3)	Length (cm)	time (h)	S (g/cm^3-cmHg)	D (cm^2/sec)
1	4.98×10^{-7}	1.58×10^{-3}	0.118	11.4	0.245	2.04×10^{-6}
2	4.29×10^{-7}	1.60×10^{-3}	0.158	24	0.248	1.73×10^{-6}
3	3.93×10^{-7}	1.55×10^{-3}	0.187	35.5	0.237	1.64×10^{-6}
4	3.86×10^{-7}	1.64×10^{-3}	0.211	48.6	0.253	1.53×10^{-6}
5	3.52×10^{-7}	1.54×10^{-3}	0.229	59.1	0.238	1.48×10^{-6}

Figure 2.3 shows the diffusion distance of the five samples tested in a dry environment whereas Figure 2.4 shows the diffusion distance in a sulfur environment saturated with water vapor. The distance that sulfur travels through the polyurethane at constant temperature is shown to be linear. The error bars depicted on each graphs represent the standard error for that set of experiments. The correlation coefficient of 0.992 represents a strongly consistent dataset.

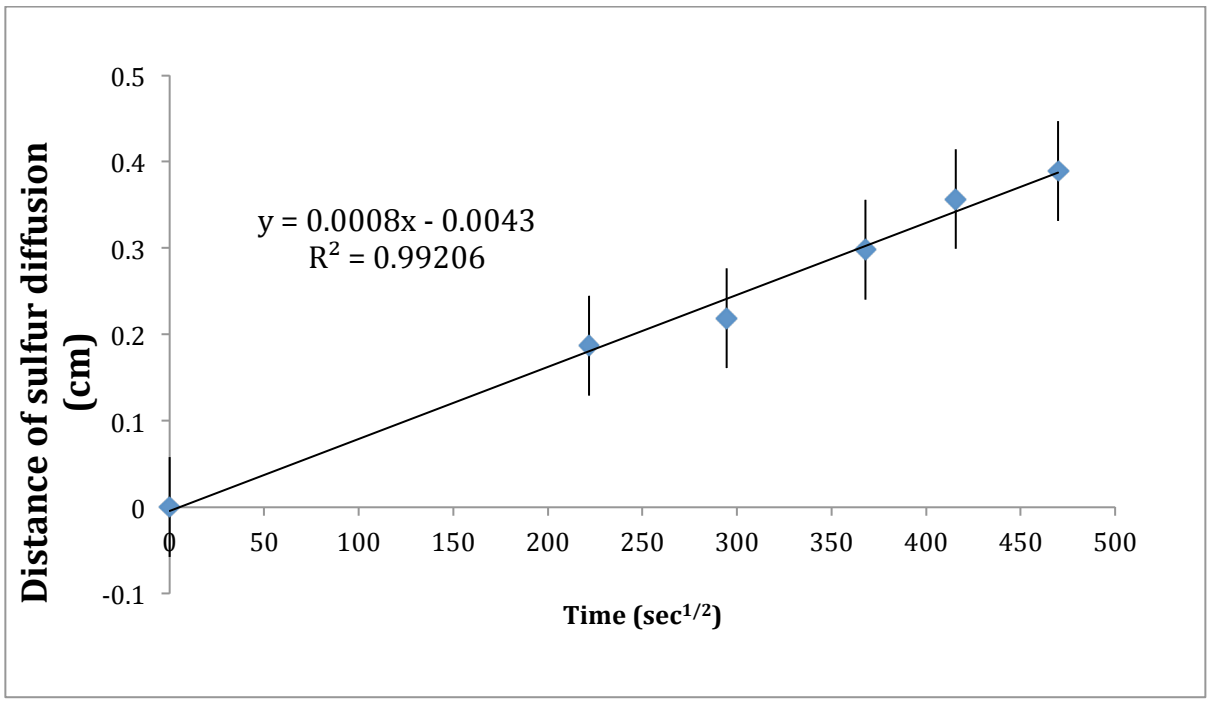

Figure 2.3: Diffusion of sulfur in polyurethane at 110°C in a dry atmosphere

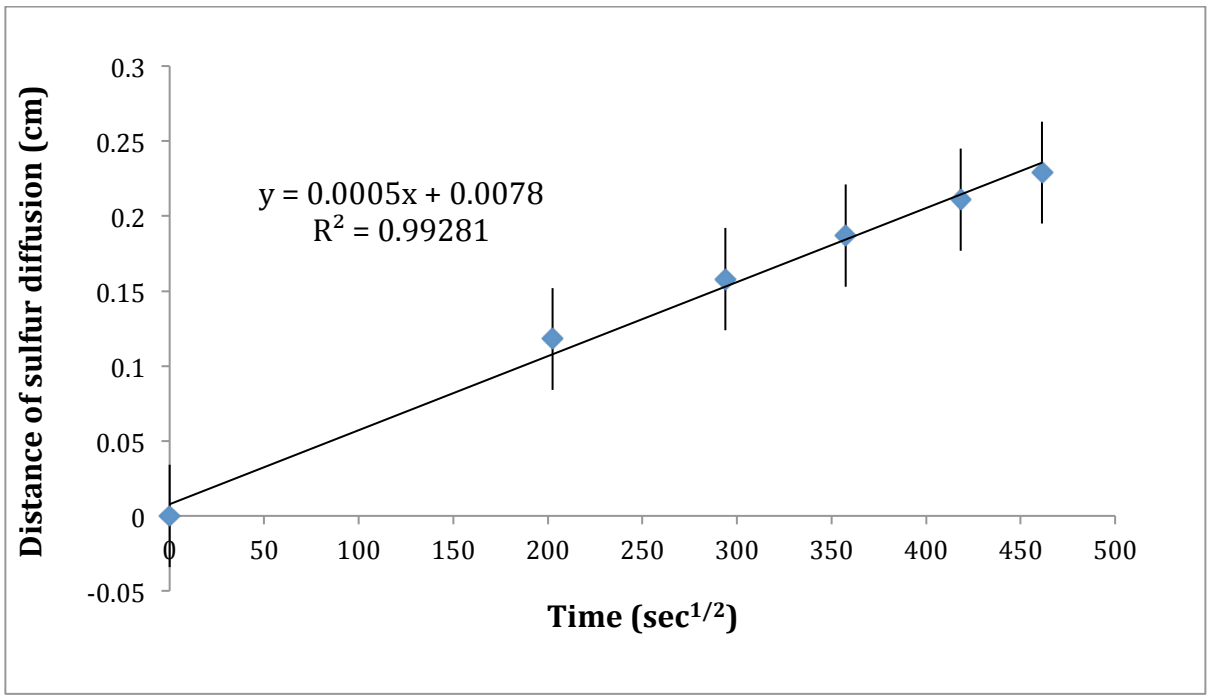

Figure 2.4: Elemental sulfur diffusion in polyurethane at 110C in a saturated atmosphere.

2.4.2 Sulfur Dioxide Experiments with Polyurethane:

Figure 2.5 shows the diffusion distance of the five samples tested in a dry environment and Table 2.4 shows all relevant parameters of the mass transport of sulfur dioxide through the polyurethane. The distance that sulfur dioxide travels through the polyurethane at constant temperature is shown to be linear, as was the case with the sulfur powder used in the first set of experiments.

Table 2.4: Calculated values for permeability, diffusivity, specific solubility, and concentration with exposure to sulfur dioxide at 110C in a dry environment.

Sample	P (g-cm/cm^2-sec-cm Hg)	C, (g/cm^3)	Length (cm)	time (h)	S (g/cm^3-cmHg)	D (cm^2/sec)
1	7.19×10^{-13}	1.73×10^{-3}	0.026	2.3	1.47×10^{-6}	4.89×10^{-7}
2	1.01×10^{-12}	1.75×10^{-3}	0.046	6.7	1.90×10^{-6}	5.26×10^{-7}
3	9.25×10^{-13}	1.80×10^{-3}	0.043	6	1.80×10^{-6}	5.14×10^{-7}
4	9.55×10^{-13}	1.72×10^{-3}	0.054	9.52	1.87×10^{-6}	5.11×10^{-7}
5	9.90×10^{-13}	1.72×10^{-3}	0.055	9.52	1.87×10^{-6}	5.28×10^{-7}

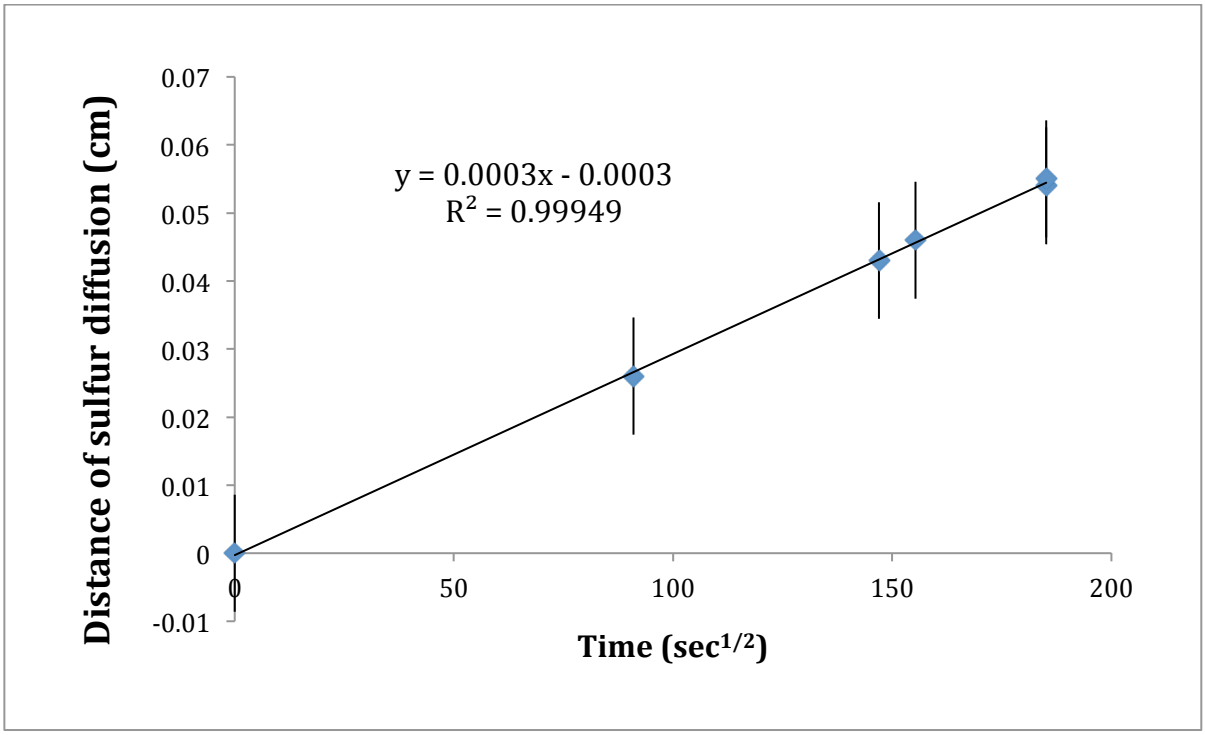

Figure 2.5: Diffusion of sulfur dioxide in polyurethane at 110°C in dry conditions.

The experiment conducted to create Figure 2.5 has two data points with the same exposure time. Mass transport in these two samples is very consistent with each other and contributes to the correlation coefficient of 0.999. Considering that the data from different time length samples correlates well together as well as is consistent with two samples with the same exposure time, we believe the data is easily repeatable.

Figure 2.6 shows the diffusion distance of the five samples tested in a humid environment. The distance that the sulfur dioxide travels through the polyurethane at constant temperature is shown to be linear. In Table 2.5 the

permeability, diffusivity, specific solubility of sulfur in polyurethane, concentration of sulfur, length traveled, and time are shown.

Table 2.5: Calculated values for permeability, diffusivity, specific solubility and concentration at 110C in a sulfur dioxide environment saturated with water vapor.

Sample	P (g-cm/cm^2-sec-cm Hg)	C, (g/cm^3)	Length (cm)	time (h)	S (g/cm^3-cmHg)	D (cm^2/sec)
1	1.17×10^{-12}	1.65×10^{-3}	0.035	8.25	4.74×10^{-6}	2.47×10^{-7}
2	1.44×10^{-12}	1.48×10^{-3}	0.046	10.4	4.25×10^{-6}	3.33×10^{-7}
3	9.11×10^{-13}	1.37×10^{-3}	0.029	6.07	3.94×10^{-6}	2.31×10^{-7}
4	1.80×10^{-12}	1.52×10^{-3}	0.067	18.2	4.38×10^{-6}	4.11×10^{-7}
5	1.55×10^{-12}	1.59×10^{-3}	0.052	13.3	4.57×10^{-6}	3.38×10^{-7}

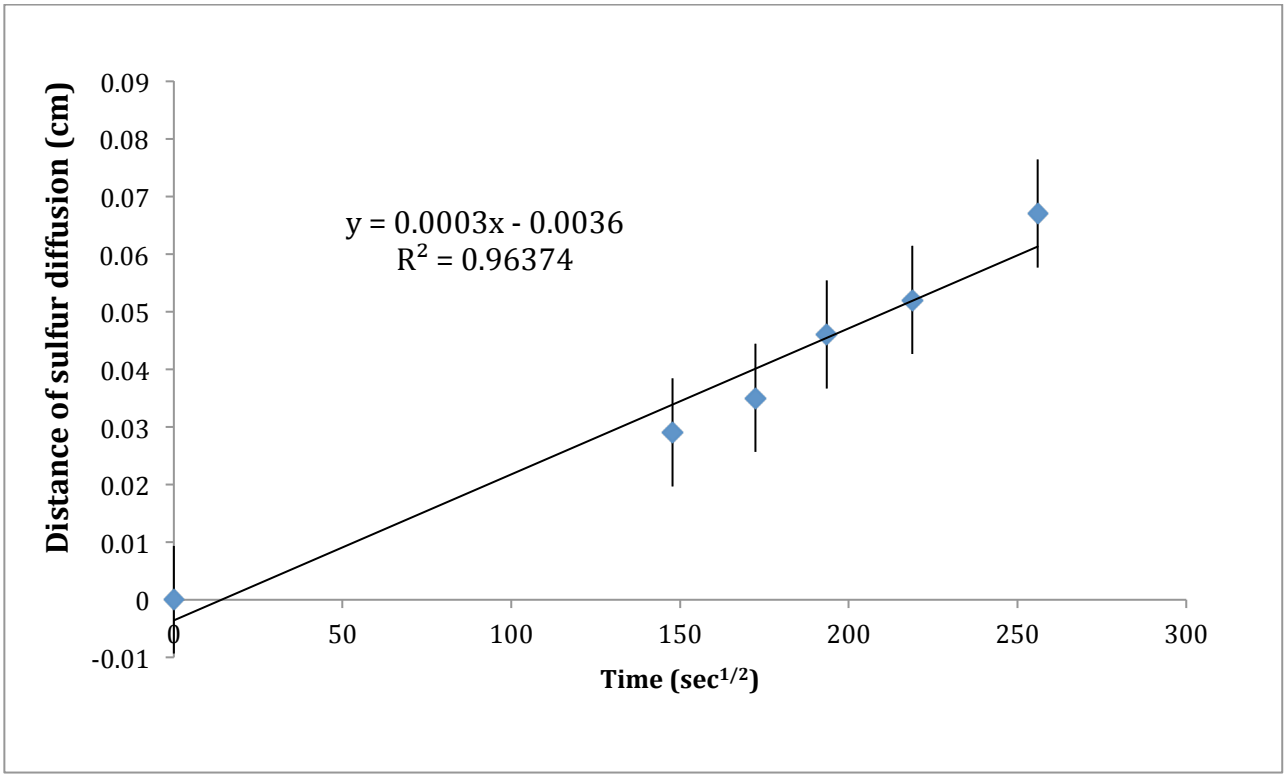

Figure 2.6: Diffusion of sulfur dioxide in polyurethane at 110°C in humid conditions.

2.4.3 Hydrogen Sulfide Experiments with Polyurethane:

The data below corresponds to the experiments performed with hydrogen sulfide. Figure 2.7 shows the diffusion distance of the five samples tested in a dry environment and Table 2.6 shows all relevant parameters of the mass transport of hydrogen sulfide through the polyurethane. Figure 2.8 shows the diffusion distance of the five samples tested in a humid environment with hydrogen sulfide. Table 2.6 shows the mass transport parameters of hydrogen sulfide through polyurethane in a humid environment. The distance that hydrogen sulfide travels through the polyurethane at constant temperature is shown in Figure 2.8 to be linear. Table 2.6 below shows the average values of permeability and diffusivity for each gas tested in both a humid and dry environment.

Table 2.6: Calculated values for permeability, diffusivity, specific solubility, and concentration in a dry hydrogen sulfide environment at 110C.

Sample	P (g-cm/cm^2-sec-cm Hg)	C, (g/cm^3)	Length (cm)	time (h)	S (g/cm^3-cmHg)	D (cm^2/sec)
1	2.43×10^{-11}	1.63×10^{-3}	0.151	7.31	4.68×10^{-6}	5.20×10^{-6}
2	1.53×10^{-11}	1.61×10^{-3}	0.183	16.8	4.62×10^{-6}	3.32×10^{-6}
3	2.13×10^{-11}	1.57×10^{-3}	0.207	15.0	4.51×10^{-6}	4.75×10^{-6}
4	2.23×10^{-11}	1.52×10^{-3}	0.168	9.25	4.38×10^{-6}	5.09×10^{-6}
5	2.14×10^{-11}	1.39×10^{-3}	0.134	5.6	4.00×10^{-6}	5.34×10^{-6}

Table 2.7: Calculated values for permeability, diffusivity, specific solubility, and concentration in a humid atmosphere of hydrogen sulfide.

Sample	P (g-cm/cm^2-sec-cm Hg)	C, (g/cm^3)	Length (cm)	time (h)	S (g/cm^3-cmHg)	D (cm^2/sec)
1	1.73×10^{-11}	1.57×10^{-3}	0.144	9	4.51×10^{-6}	3.84×10^{-6}
2	1.56×10^{-11}	1.54×10^{-3}	0.168	13.3	4.44×10^{-6}	3.52×10^{-6}
3	1.21×10^{-11}	1.12×10^{-3}	0.121	6.5	3.21×10^{-6}	3.75×10^{-6}
4	1.72×10^{-11}	1.90×10^{-3}	0.160	13.5	5.45×10^{-6}	3.16×10^{-6}
5	1.95×10^{-11}	1.53×10^{-3}	0.102	3.9	4.39×10^{-6}	4.44×10^{-6}

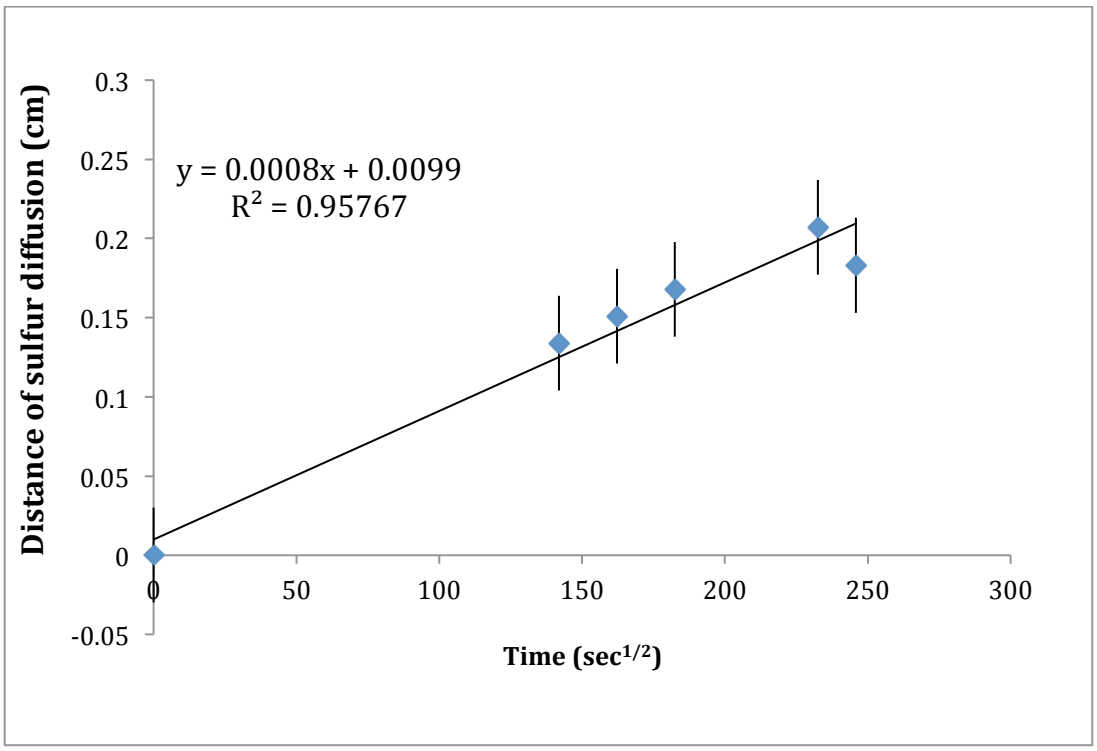

Figure 2.7: Diffusion of hydrogen sulfide in polyurethane at 110°C in dry conditions.

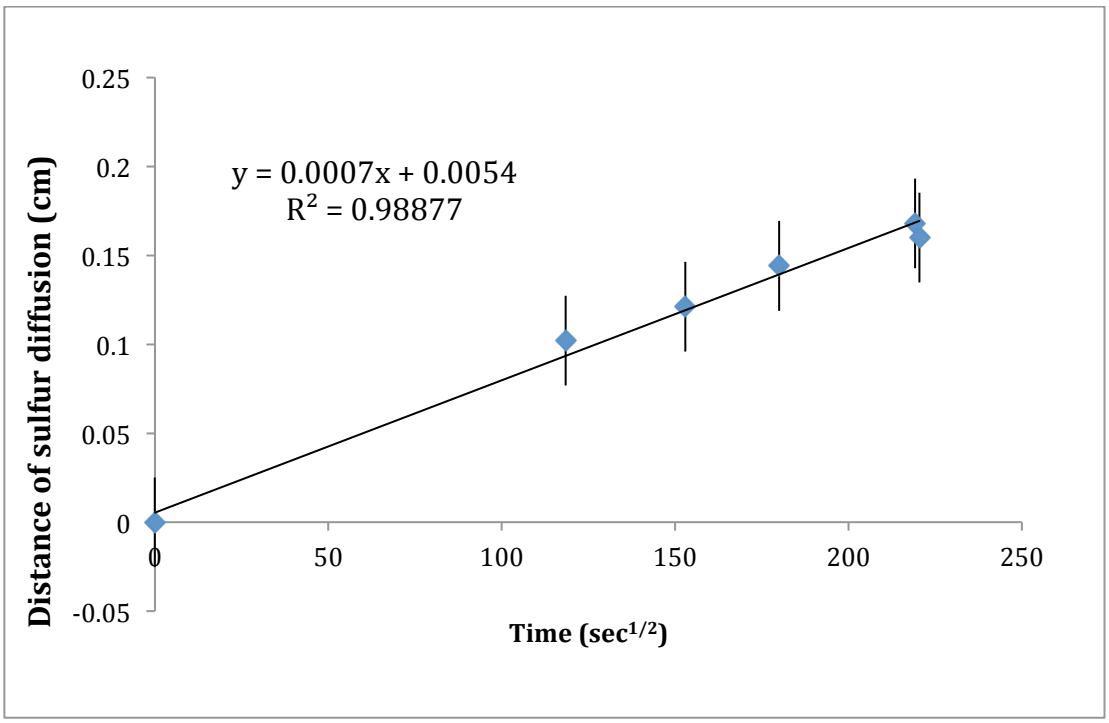

Figure 2.8: Diffusion of hydrogen sulfide in polyurethane in humid conditions at 110°C.

This data is consistent with the other two sulfur compounds tested in that while the mass transport occurred at a different rate the same linear trend is observed. All of the previously presented data appears to be easily repeatable and correlate well within the respective group of samples.

Table 2.8 provides a concise presentation of averages of the permeability and diffusivity calculated from the experiments conducted with sulfur powder, sulfur dioxide and hydrogen sulfide in both a dry and humid environment.

Table 2.8: Average values for permeability, and diffusivity in a variety of environmental conditions.

Experiment	Permeability (g-cm/cm^2-sec-cm Hg)	Diffusivity (cm^2/sec)
Sulfur vapor, dry	9.50×10^{-7}	4.01×10^{-6}
Sulfur vapor, humid	4.12×10^{-7}	1.68×10^{-6}
Sulfur dioxide, dry	9.19×10^{-12}	5.13×10^{-7}
Sulfur dioxide, humid	1.37×10^{-12}	3.13×10^{-7}
Hydrogen sulfide, dry	2.09×10^{-11}	4.74×10^{-6}
Hydrogen sulfide, humid	1.63×10^{-11}	3.74×10^{-6}

It is easy to see that the results from the sulfur dioxide and hydrogen sulfide experiments had a lower correlation coefficient than the sulfur powder. The increase in variation can be attributed to the short diffusion distance that is observable using the current model. A more sensitive model could decrease the variation observed in the results for the sulfur dioxide and hydrogen sulfide experiments. While the results for those experiments exhibited more variation than those of the sulfur powder experiments, we do not feel as though it negatively impacts the results. Considering the correlation coefficient for the

experiment with the largest variation(hydrogen sulfide-dry environment) was still over 0.95, a more sensitive model is not a necessity. The diffusion of sulfur dioxide or hydrogen sulfide is not observable after approximately the first millimeter of polyurethane because of the anhydrous environment inside the polyurethane. Without the ability to track further diffusion with the method employed, a slight increase in the amount of variance was encountered and was due to human error when measuring samples. This error was encountered even with the help of a microscope. Neither sulfur dioxide nor hydrogen sulfide react with silver in a purely anhydrous environment. The sulfur dioxide or hydrogen sulfide must first react with water to form sulfuric acid. Sulfur vapor does not follow the same mechanism of reaction with silver; this allows it to be observable throughout the entire polyurethane sample.

While there are a number of factors that affect the rate of diffusion of one material/fluid through another material/fluid, two of the main factors are molecule size and electrical charge on each molecule. For example with two fluids, one nonpolar, and one polar, there is negligible diffusion of the fluids. The opposite is true if the fluids are either both polar or both nonpolar. When examining the diffusivity of gases through solids, as is the case with the sulfur compound/polyurethane experiments, the size of the gas molecule will also have a significant effect upon the rate of diffusion. The sizes and polarities of each compound are given in Table 2.9.

Table 2.9: Sizes and dipoles of sulfur compounds studied (data retrieved from the NIST WebBook).

Molecule	Hypotenuse of molecule (Å)	Dipole (Debye)
Sulfur vapor	2.04	0 (no dipole)
Hydrogen sulfide	1.91	0.970
Sulfur dioxide	2.47	1.63

The difference in diffusion rates is due to a reduction in possible diffusion sites that can accommodate the larger molecules. We observed that hydrogen sulfide had the highest diffusion rate through the polyurethane with a rate of 4.74×10^{-6} cm^2/sec, and it is believed that this is due to its relatively small size in relation to sulfur dioxide and sulfur vapor. As a gas, sulfur vapor forms several allotropes, one of which is S_2. Since sulfur forms an S_2 allotrope, its size is between both hydrogen sulfide and sulfur dioxide[6].

2.4.4 Transport Modeling:

To tie the results of the experiments to a real world application such as a potting material for electronics, some basic modeling was performed using the experimental data collected. The analysis is conducted on the basis of a worst-

case scenario similar to that tested where the polyurethane is exposed to a saturated sulfur environment. For a real environment where the sulfur concentration is much lower and many other factors are at play the lifespan or mass transport times will likely be much different. The model still has value as it gives a good idea of how quickly sulfur compounds diffuse through polyurethane; illustrating the need for a potting material with a much lower permeability to these compounds to be identified or developed.

Case 1: Environmental conditions with elemental sulfur is present which is located in a desert location the potting material is 5cm thick on the surface of the electronic device. How much time passes before the device begins interacting with the sulfur vapor in the atmosphere.

$$\tau = \frac{l^2}{6D} \qquad 4$$

Based upon this model, the sulfur vapor would begin to come into contact with the silver in the circuit in 12.02 days. Where t is the time the sample was exposed to the sulfur environment, sec; l is the distance traveled by the sulfur through the sample, cm; and D is the diffusivity of sulfur in polyurethane, cm^2/sec. As can be seen, this is based upon a worst-case scenario as the high temperature, pure sulfur environment, and the low humidity only serve to increase the diffusion rate.

Case 2: The electronic device must resist any corrosion for a period of 10 days in a dry environment while exposed to hydrogen sulfide. What thickness will insure that the device will still be active after this period.

$$l = \sqrt{6\tau D} \qquad 5$$

Rearranging Equation 4, the required thickness of the polyurethane can be calculated. The silver would withstand being acted upon by the sulfur vapor if it was thicker than 4.56cm.

2.5 Conclusions:

The data presented above is summarized in the following points.

- Hydrogen sulfide had the highest diffusivity, 4.74 $x10^{-6}$ cm^2/sec, through polyurethane, followed by sulfur vapor, 4.01 $x10^{-6}$ cm^2/sec, and sulfur dioxide exhibited the smallest diffusivity of 5.13 $x10^{-7}$ cm^2/sec
- A humid environment greatly slowed the transport of the sulfur compound by 58.1% (sulfur vapor), 38.9% (sulfur dioxide), and 21.1% (hydrogen sulfide), because of competition for active sites.
- The rates of transport appear to be attributed to the size of the molecule diffusing. For example hydrogen sulfide is the smallest molecule with a 1.91Å hypotenuse. Assuming environmental conditions are constant.
- Transport rates were demonstrated to be linear in all cases tested. As seen in Figures 2.2; 2.4-2.10.

The experiments show the transport properties of sulfur and sulfur dioxide in polyurethane. This data can be used to estimate the amount of time for sulfur or sulfur dioxide to transport through a distance of polyurethane. The diffusion of sulfur in a humid environment is interesting because it is significantly lower than that of a dry environment, 58.1% (sulfur vapor), 38.9% (sulfur dioxide), and

21.1% (hydrogen sulfide). This is due to the availability of diffusion sites on the polyurethane and the fact that some are taken by water essentially out-competing the sulfur for entry points into the polyurethane. A detailed explanation and experimental investigation of this phenomenon can be found in Mercier et. al[5] and many other sources in the literature.

It is believed that the size of the molecules investigated accounts for the differences in diffusion rates of sulfur vapor and the two sulfur compounds through polyurethane. A material with a higher density and much lower porosity would cause a significant improvement in the ability to protect any electronics from sulfur corrosion and failure.

2.6 Acknowledgment:

We acknowledge General Electric (GE) for their support of this project.

2.7 References:

[1]Sinclair J.D. Tarnishing of Silver by Organic Sulfur Vapors: Rates and Film Characteristics, *j. electrochem. Soc.* 1982, 33-40.

[2]G. Digiacomo, and E. Spaulding, A Method for Determining the Permeability and Solubility of Sulfur in Poly(dimethylsiloxane) (RTV), *Journal of Applied Polymer Science*, (1979), 23, 261-274.

[3]Gehman S. D. and Auerbach I. Tracer method for sulfur solubility and diffusivity in rubber, *Analytical Chemistry,* 1954, 26, 685-690.

[4]Susko, J. R. and Berry, B. S. Solubility and Diffusion of Sulfur in Polymeric Materials, *IBM J. RES. Develop.* 1977, 174-189.

[5]Mercier, R.; Espuche, E.; Piroux, F. The effects of humidity on gas transport properties of sulfonated copolyimides, *Journal of membrane science.* 2003, 115-122.

[6]B. Meyer. Elemental Sulfur *Chemical Reviews*, (1976), 76, 367-388.

Chapter III: Characterization of Polyphenylquinoxaline as a Sacrificial Heat Exchanger Coating

3.1 Abstract:

Polyphenylquinoxaline (PPQx) was investigated as a sacrificial heat exchanger coating. The coating exhibited a thermal conductivity of 0.1742 $W(m^2K)^{-1}$ and adhesion strength of 1.213lbs/mm^2. Molecular weight was 65,000g/mol using an Ubbleholde viscometer. When coated onto stainless steel the polymer thickness was 0.97-1.03mm. In all experiments the polymer showed excellent thermal stability including when heated and cooled repeatedly. The properties exhibited by the polymer are required for a coating exposed to high temperature, high pH stream with high suspended solids.

3.2 Background:

Polyphenylquinoxaline (PPQx) is a highly aromatic, six-membered ring heterocyclic polymer. PPQx has been investigated and characterized as a high glass transition polymer with excellent high temperature stability[1,2]. Having strong high temperature stability makes PPQx a candidate for a heat exchanger coating because it will be stable under high temperature and pH conditions. The quinoxaline group is a double ring structure containing an aromatic ring fused to a pyrazine ring at two adjacent carbons. Its chemical structure is shown in

Figure 3.1. PPQx is synthesized from amino-aromatic aldehyde and bisketomethylene groups.

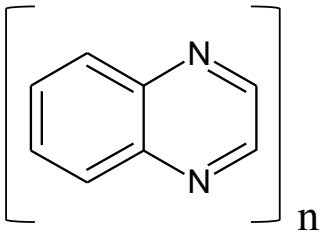

Figure 3.1: Quinoxaline chemical structure.

Heat exchangers generally operate in harsh conditions, and their materials must be able to withstand repeated cooling and heating cycles. These materials must also hold up against abrasion if solids or solid containing fluids are being heated or cooled. Heat exchangers also experience fouling, scaling, and corrosion in many industrial settings[3]. Fouling can occur when solids from the process stream begin to deposit upon the surface of the heat exchanger or other unit operation. This can be highly detrimental to the operating efficiency of the heat exchanger due to the extra thickness for conduction to occur across. Scaling is a similar process that occurs when impurities are precipitated from the process stream onto the walls of the piping[3]. These solids can act as an insulator similar to fouling however a Teflon surface, that could inhibit fouling would have no effect on the presence of scale. Teflon is commonly used for an antifouling coating in heat exchangers due to the low surface energy of the polymer creating in essence a ‘slippery’ surface. Coatings are extensively used to attempt to mitigate the effects of fouling and corrosion, and these coatings are generally polymers[3,4]. Unfortunately most polymers have low thermal

conductivity, compared to metals, generally less than 1 W/(m^2 K). To achieve efficient heat transfer, free electrons must be present to aid in conductive heat transfer. PPQx has been studied by as an electron transport material for polymer light emitting diodes[5], but it displayed unipolar electron transport, which is not ideal for electroluminescent.[5] With the application of heat transfer unipolar electron transport is not a concern as the energy needs only to flow in one direction for efficient operation. In order for the heat exchanger to operate optimally the heat needs only to flow in one direction, either into or out of the process stream. Given the result of unipolar electron transport PPQx appears to be a strong candidate for a heat exchanger coating from the case of thermal conductivity. The low thermal conductivity of polymer (Teflon) is shown in Table 3.1 below:

Table 3.1: Thermal conductivities of common materials in W(m^2K)$^{-1}$ [3]

Aluminum	Carbon Steel (0.5%C)	Carbon Steel (1.5%C)	Teflon
167	53.6	36.35	0.25

Considering the low thermal conductivity of polymers in relation to those of metals, as shown in Table 3.1, it is possible to add metal powders to the polymer coating to assist with the heat transfer. Two candidates for this are silicon carbide and tungsten. Silicon carbide has a crystal lattice structure composed of

tetrahedral carbon with silicon atoms attached. This structure yields a strong and hard material, silicon carbide is also not affected by any acids, alkalis, or molten salts up to 800^{o}C[6]. Tungsten has the lowest thermal expansion of any pure metal as well as a high melting point of 3422^{o}C[7]. When designing a heat exchanger, pure aluminum would be one of the best choices but when faced with fouling, scaling or abrasion it becomes necessary to use a polymer coating. The coating can help mitigate these effects or has a lower cost to replace rather than replace the entire heat exchanger.

This research investigates the potential for a polymer coating applied in a heat exchanger. The thermal conductivity of PPQx, thermal stability, adhesion properties, and possible metal fillers are investigated.

3.3 Experimental:

3.3.1 Materials:

1,4 bisbenzil, m-cresol, 3'-diaminobenzidine (aromatic tetramine-DAB) were purchased from Sigma Aldrich and TCI America used as received without further purification. Multipurpose stainless steel sheet (type 304) #2B Mill Finish, 0.36" thick, 12" x 12" was purchased from McMaster-Carr.

3.3.2 Synthesis of PPQx:

An equimolar amount of 1,4 bisbenzil and 3,3'-diaminobenzidine (aromatic tetramine) are dissolved in m-cresol (solvent) and reacted at 100°C in a nitrogen environment. After 24 hours, the solution is cooled at room temperature and then precipitated in methanol. Yellow precipitate is obtained (polymer). The polymer is then washed several times with ethanol to remove the remaining solvent and un-reacted monomer. The polymer is then dried in a vacuum oven at 40°C for 24 hours. Figure 3.2 shows the mechanism of the reaction of PPQx[8].

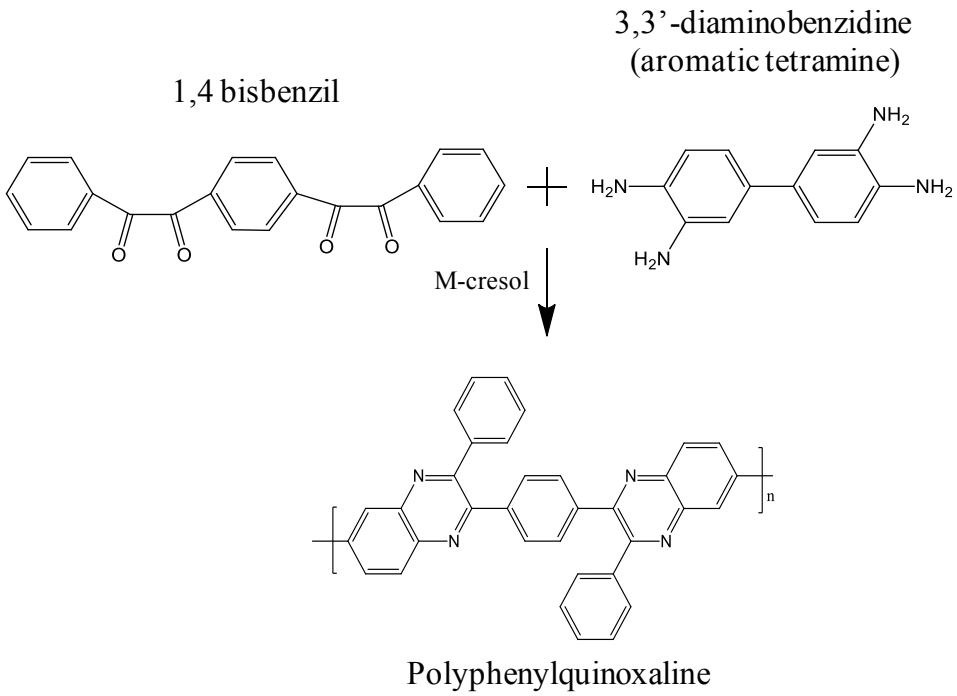

Figure 3.2: Mechanism of PPQx reaction.[8]

3.3.3 Surface Preparation of Stainless Steel (SS) Coupons

Stainless steel sheet is cut into square coupons (5 cm x 5 cm). The SS coupons are surface roughened with a Dremel tool using a sanding drum 430. The roughed SS coupons are washed with soap water to remove all the grease and/or oil and finally air dried.

3.3.4 Surface Coating of PPQx on the SS Coupon

Dried PPQx is dissolved in m-cresol. The viscous solution is then used to coat the surface of the SS coupon. The first step is to coat a thin layer (dilute polymer solution) of the polymer on the surface of the SS coupon under vacuum and heating it up to 80^{o}C for 24 hours to ensure that all m-cresol is driven off.

3.4 Characterization:

3.4.1 Polymer Molecular Weight:

A Ubbelohde viscometer is used to determine the synthesized polymer molecular weight. The ratio of the polymer solution viscosity to the solvent viscosity is used to determine the molecular weight of polymer. Ostwald or Ubbelohde viscometers are used to measure the viscosity of both the polymer solution and solvent. The viscosity measurement is done in the water bath to keep the temperature constant at 25^{0}C, as the viscosity is a function of temperature[9,10,11,12].

3.4.2 Mechanical Properties of the Polymer:

The mechanical properties of the polymer are characterized using a Perkin-Elmer dynamic mechanical analyzer 7e (DMA). The thin film polymer sample is exposed to tension as a function of the strain. Increasing the amplitude of the tension applied the upper limit of PPQx's stress-strain can be determined.

3.4.3 Evolved gas analysis/pyrolyzer system (EGA/PY):

Additional characterization using EGA/PY is done in order to characterize the thermal stability of the PPQx. Pyrolysis is a thermochemical decomposition of organic material at elevated temperature in the absence of oxygen. EGA/PY tests the gases released from the sample as it is heated to high temperatures. The gases given off will be the decomposition method for the compound. EGA/PY will give insight into which portions of the polymer are degrading and the temperatures at which they decompose. This characterization is done in collaboration with Frontier Lab, Antioch, CA.

3.4.4 Heat treatment testing:

The coated SS coupons are tested in order to determine whether the coated samples could withstand an elevated temperature of 200^{o}C . The coupons are tested in a Parr Reactor for 6-7 hours at high temperature (200^{o}C) and pressure (30 bar). If the coating is still intact and attached to the surface of the SS coupon the experiment is considered successful, oxidation will be observed due to a darkening of the color of the coating.

3.4.4 Durability/Shear testing:

The coated SS coupon is dipped into a silicone oil bath at 200°C for 5 minutes and then removed to room temperature for 5 minutes; this constituted one cycle.

Shear testing is done using a Com-Ten Industries series 95. Samples are shear tested after thermal cycling to determine if there is any effect on the adhesion of the PPQx coating to the SS coupon. The coating is applied to two coupons in an overlapping arrangement. Samples are shown in Figure 6 of the Results/Discussion. The sample is then pulled from each coupon to determine the amount of adhesive force exhibited by the coating onto the SS coupon.

3.4.6 Thermal conductivity:

SS coupons with one , two and three layers of PPQx are tested for thermal conductivity. The testing is done over a range of temperatures from ~40 ^{o}C - 100^{o}C. The thermal conductivities are measured with an Omega Engineering, Inc Model DP3520-PA heat flux sensor.[12]

The thermal conductivity is calculated using Equation 1:

$$Q = \frac{k}{\Delta L} \times \Delta T \quad (1)$$

In Equation 1, Heat flux is Q (W/m^2), ΔL is the thickness of the sample (m), ΔT is the temperature difference between the two layers, and k is the thermal conductivity in (W/(m^2 K)$^{-1}$).

3.5 Results and Discussion:

3.5.1 Molecular Weight (MW)of Polymer:

The molecular weight of PPQx was characterized using a Ubbelohde viscometer as discussed in Section 3.1. A polystyrene standard with various molecular weights was used. Polystyrene standards with 65,000, and 170,000 molecular weight were used to measure the intrinsic viscosity vs. MW. The intrinsic viscosity vs. MW data shows that the viscosity of the sample is close to

the 65,000 polystyrene standard because the intrinsic viscosity is 0.292. Table 3.2 shows the intrinsic viscosity data and molecular weight of the standard. A third standard molecular weight was obtained however, the result did not seem accurate and as a result was not included in the molecular weight analysis of PPQx.

Table 3.2: Intrinsic viscosity of polystyrene at different molecular weights.

$\eta_{intrinsic}$	Molecular weight
0.371	65,000
0.8055	170,000

3.5.2 Mechanical properties of polymer:

Dynamic Mechanical Analysis (DMA) was used to measure the stress and strain of the PPQx coating which is shown in Figure 3.3. Based upon the figure, it is clear that polyphenylquinoxaline has high elasticity (100% strain at 9700kPa stress applied). In an abrasive stream the high elasticity of PPQx is highly desirable because instead of cracking when placed under stress the coating has a high likelihood of reacting to the stress and recovering.

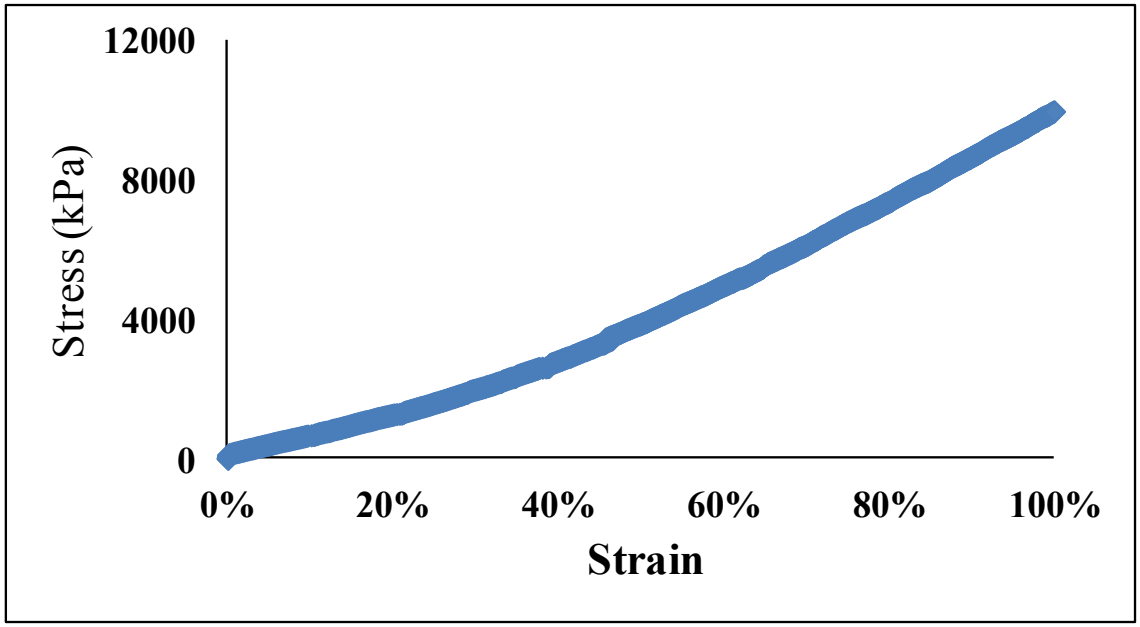

Figure 3.3: Stress as a function of strain for PPQx

3.5.3 Evolved gas analysis/pyrolyzer system (EGA/PY):

EGA/PY was done in order to characterize the thermal stability of the PPQx.[1] Pyrolysis is a thermochemical decomposition of organic material at elevated temperature in the absence of oxygen. Figure 5 shows the thermogram of a PPQx sample. From the thermogram, the sample shows two major features, i.e. the first feature is the volatile component (<350^{o}C) and *the second feature is the base polymer being pyrolyzed at temperatures of 500-700^{o}C (peak at ± 600^{o}C)*.. This demonstrates that PPQx has a good thermal stability, which is

[1] This characterization was done in collaboration with Frontier Labs, Antioch, CA

important for its use as a heat exchanger coating. We believe that the high thermal stability is due to the aromatic nature of the polymer. PPQx has also been shown to have excellent heat stability in the literature[11].

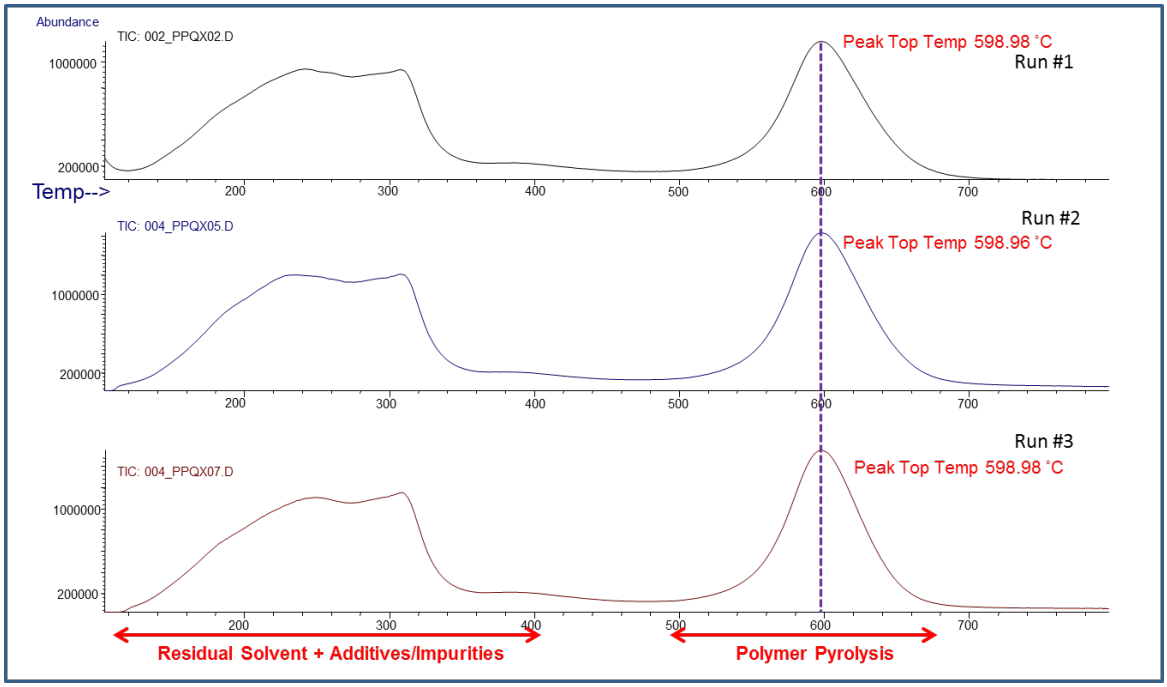

Figure 3.4: EGA thermogram of PPQx.

3.5.4 Heat Treatment Testing:

The surface coated SS coupons were tested under high pressure and temperature (30 bar and 200^{o}C) using a Parr reactor in order to see if the adhesion between the PPQx and the SS coupons was satisfactory under the desired conditions. Two samples of coated SS coupons were tested for 7 hours and the coating on the coupons was still intact. A second test was done on three

samples of coated SS coupons in silicone oil at 200^{o}C for 72 hours and the coatings were unaffected, as shown in Figure 8. The thickness of the coating was between 970 – 1030 microns (0.97-1.03mm) with an average mass of PPQx used was 0.2 grams. The composite coated SS coupon was tested in silicone oil at 100^{o}C for 24 hours and the coating was intact. The composite of SiC/PPQx and W/PPQx at ± 36wt% of additives after being tested in silicone oil at 200^{o}C for 72 hours. The coating was still firmly attached after the 72 hour test. This is a very encouraging result as it shows the composite did not adversely affect the adhesion of the polymer to the stainless steel coupon. The composite was chosen because of the high thermal stability of silicon carbide and the thermal conductivity of tungsten[6,7].

3.5.5 Mechanical Testing:

Shear testing was performed on samples with the compression-tensile instrument. The average adhesion of the untreated samples for the experiments is 1.213lbs/mm^2. After thermal cycling it can be seen in Table 3.3 that there is a slight downward trend in the adhesion of the sample to the stainless steel coupon. This is expected due to the partial oxidation of the polymer coating. The partial oxidation can explain the lack of a significant downward trend in the strength of adhesion, as the amount will vary per sample. The PPQx does not lose significant adhesion strength to the stainless steel even after a large number of thermal cycles. The variance observed in Table 3.3 can be attributed to the

partial oxidation as the sample did not oxidize evenly and certain areas experienced more at different times. This effect can be seen in Figure 3.5, as the samples experience more cycles and more oxidation the partial oxidation becomes much more even.

Table 3.3: Shear strength of PPQx to SS after thermal cycling.

Sample	Average Adhesion (2 samples) (lbs/mm^2)
15 cycles	1.879
25 cycles	1.537
35 cycles	1.344
45 cycles	1.612
55 cycles	1.615

Figure 3.5 shows the coupon before and after 15, 25, 35, 45, and 55 cycles. It can be seen that the color of the sample became darker as the durability tests progressed. Any darkening is the result of the partial oxidation of polymer. The partial oxidation of the polymer coating did not negatively impact the adhesive properties of the polymer to the stainless steel.

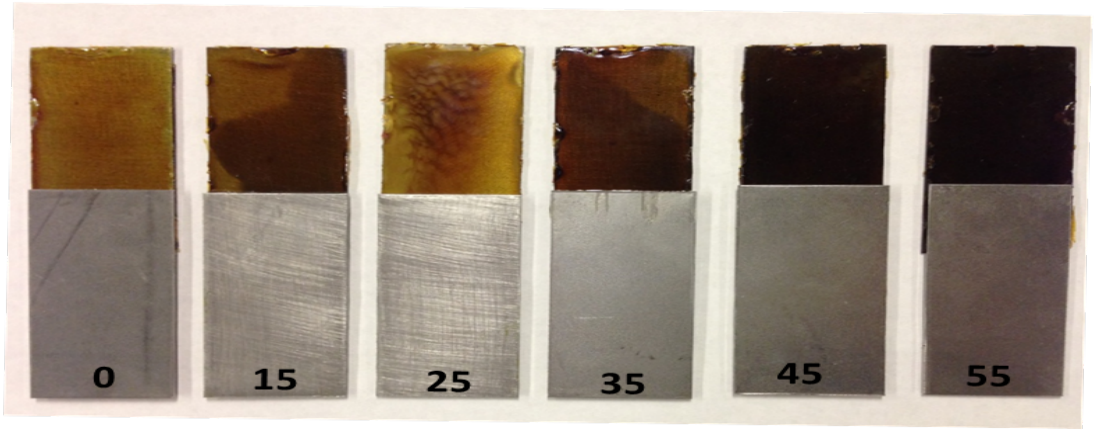

Figure 3.5: SS coupon before (0) and after cyclic testing for 15, 25, 35, 45, 55 cycles.

Figure 3.6 shows the failure of the sample when exposed to increasing force, all samples tested exhibited similar failure patterns. No partial failure was observed. The failure pattern below is consistent with a complete failure of the sample as the force decreases at 0.045 inch. It would be much less drastic with a partial failure of the adhesion of the polymer to the stainless steel coupon.

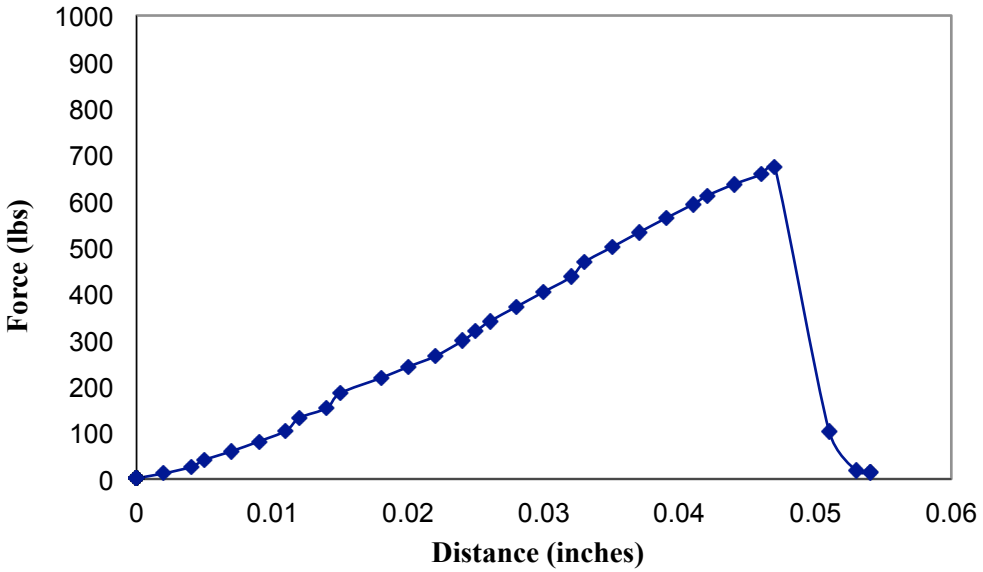

Figure 3.6: Shear test data for a PPQx sample exposed to 55 thermal cycles.

3.5.6 Thermal Conductivity:

The thermal conductivity of PPQx on stainless steel decreases with the number of layers over the temperature range of ~40 ^{o}C -100^{o}C. Figure 3.7 shows the average thermal conductivity for samples with different numbers of layers of PPQx. The average thickness per layer is 1mm. Figure 3.7 shows that there is a clear trend of an increased resistance to heat transfer as the thickness of the polymer is increased on the surface of the stainless steel. While this provides reduced heat transfer, the extra thickness of polymer is useful to provide increased abrasion resistance. The average heat transfer coefficient for the PPQx coating is low even when compared to that of Teflon shown in Table

3.1. Figure 3.7 below shows the trend of the thermal conductivity of a sample with two layers of polymer present.

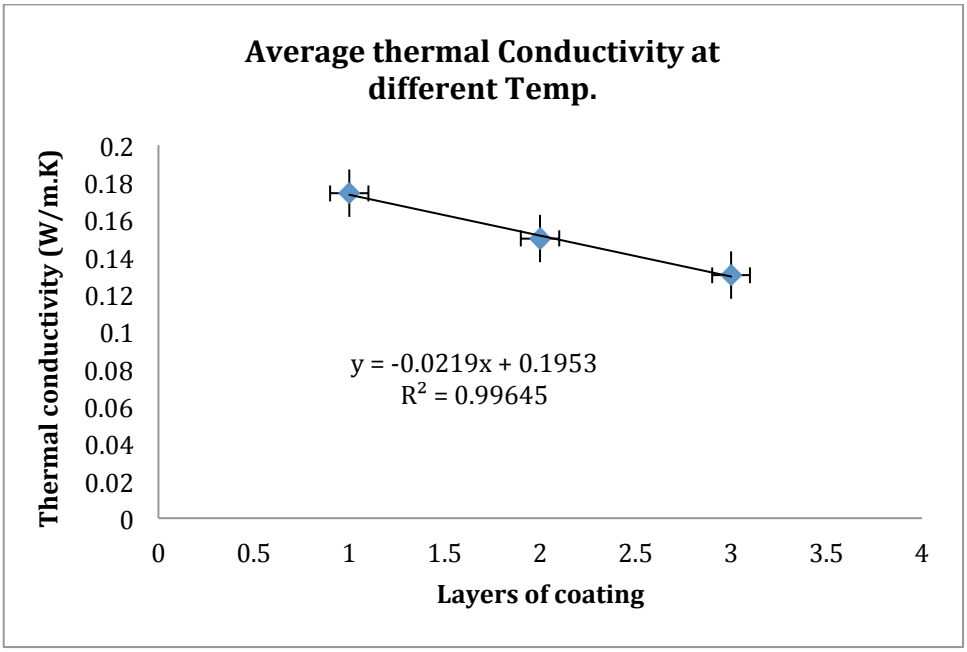

Figure 3.7: Thermal conductivity of PPQx with different coating thicknesses.

The thermal conductivity of PPQx was experimentally shown to be consistent over the range of 40^0C – 100^0C[12]. Higher temperature testing was not done as a result of safety concerns with the current experimental test station. The thermal conductivity of the polymer is expected to be roughly constant over the desired temperature range.[13]

3.6 Conclusions:

In this work polyphenylquinoxaline (PPQx), a high glass transition polymer with excellent thermal stability was investigated and characterized for use as a sacrificial heat exchanger coating. The coating would be ideal for a high solids stream as the stress-strain and adhesive properties were favorable to this application. This work supports the use of PPQx in heat exchanger applications for the following reasons:

a) Thermal conductivity of 0.1742 W/m K which is constant over the temperature range of 45 ^{o}C -100^{o}C.
b) The polymer performed well when exposed to heating and cooling cycles as well as withstanding high pressure (30bar) and temperature (200^{o}C).
c) EG/PY analysis showed that the base polymer did not pyrolyze until exposed to a temperature of 600^{o}C.

These results are promising for the PPQx coating in a high temperature, high pH, high solids stream heat exchanger.

3.7 Acknowledgements:

Dan Kappes and Dustin Albin at Kappes-Cassidy Associates are acknowledged for technical input and support for this project.

3.8 References:

[1]Economopoulos, S. P., Andreopoulou, A. K., Gregoriou, V. G., and Kallitsis, J. K., J. of Macromolecular Science, Vol. 43, pp. 977 – 988, 2006.

[2] Stille, J. K. and Williamson, J. R. (1964), Polyquinoxalines. J. Polym. Sci. A Gen. Pap., 2: 3867–3875. doi: 10.1002/pol.1964.100020904

[3]Kukulka, D.; Leising, P. Applied Thermal Engineering, Vol 30, pp. 2333-2338,2010

[4]Fedrizzi, L. Andreatta, F. Paussa, L. Deflorian, F. Maschio, S. Progress in Organic Coatings, Vol 63, pp. 299-306, 2008.

[5]O'brien, et. al. Applied Physics letters 69, 881 (1996)

[6]Harris, G Properties of Silicon Carbide, 1995

[7]Lassner, E. Schubert, W-D. Tungsten: Properties, Chemistry, Technology of the Element Alloys, and Chemical Compounds 2012

[8] Y. Cui, Z. Xuejun, S. A. Jenekhe. *Macromolecules*, Vol. 32, pp. 3824-3826, 1999.

[9] I. Pramudya, I. Adi Setiawan. Effect of NaOH Concentration and Agitation on the Degree of Deacetylation of Chitosan from Crab Exoskeleton. University of Surabaya, Indonesia, 2007.

[10] P. Russo Intrinsic Viscosity, 2008.

[11]Hendricks, C. L. Hill, S. G. Evaluation of High Temperature Structural Adhesives for Extended Service. 1984

[12]Experiment performed by Ying Liu.

[13]C. Y. Ho, R. W. Powell, P.E. Liley; Thermal Conductivity of the Elements, J.Phys.Chem. 1972.

Chapter IV: Deoxygenation of a Basic Cyanide Solution

4.1 Abstract:

Membrane contactors are generally used to add or remove dissolved from water or amine based solutions. We have explored the use of a membrane contactor to remove dissolved oxygen from a 300ppm sodium cyanide solution with a pH of 10.5. The membrane contactor chosen, Liquicel 2.5x8 had a maximum gas flux of 0.0588gO_2/m^2□min. The results indicate that the cyanide solution had no adverse effect upon the operation of the membrane and it operated at a similar efficiency to water.

4.2 Background:

There are many ways to remove dissolved gases from solution; some are more easily translated to an industrial setting. In a lab scale setting a solution can be degassed by using a freeze, thaw, freeze process, while effective at removing gases this is difficult and energy intensive to perform on a large scale. Membrane degasification is effective as a continuous process whereas a freeze, thaw, freeze is a batch process. Membrane degasification has the advantage to remove all gases by applying a vacuum to one side of the membrane. Another way to remove an unwanted gas from a solution involves, flowing the inert gas in a counter current process to the liquid side of the membrane. Figure 4.1 shows the process by which a liquid stream is degassed in a membrane contactor.

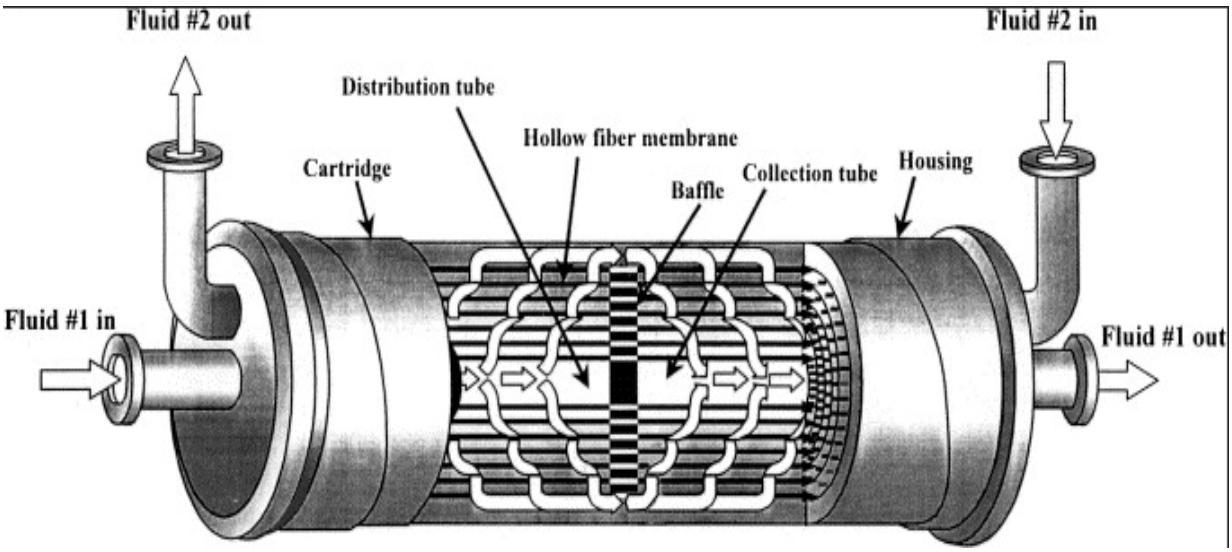

Figure 4.1: Fluid flow through a membrane contactor.[1]

Membrane contactors are versatile in their construction and are able to be created for small laboratory scale systems as well as industrial scale systems processing in excess of 2,000 gallons per minute.[1] The membrane is made out of polypropylene, a hydrophobic polymer, and the pores in the membrane are ~0.05 microns. Water or other polar solutions cannot pass through the pores thus allowing a liquid and gas interface to be created. So long as the liquid and gas sides remain separate the membrane will operate. However, as soon as the liquid is forced through the pores of the membrane, the membrane is then considered wetted and will cease to function as designed. Using the Young-Lapace equation for hydrophobic membranes, the breakthrough pressure can be calculated[1].

$$P = -2\sigma cos\frac{\theta}{r} \qquad [1]$$

In Equation 1, P is the breakthrough pressure, θ is the contact angle, σ is the surface tension of the liquid, and r is the radius of the pores in the membrane. The membrane contactors rely upon Henry's law for the driving force of mass transfer of gas out of the solution. Henry's law states that the amount of gas that will dissolve into water at equilibrium is proportional to its partial pressure in the vapor phase in contact with water. This relationship is shown in Equation 2 where p is the gas partial pressure, H is henrys' law coefficient, and x is the concentration of dissolved solute[2].

$$p = Hx \qquad [2]$$

To create the driving force of partial pressure differences Liqui-Cel® membrane contactors use either a vacuum or a nitrogen purge. This method allows for the membrane contactor to achieve dissolved oxygen levels of 1.0ppb. The membrane contactors can also be used to increase the concentration of gases in solution in the case of CO_2 injection at a Pepsi plant to carbonate soft drinks[2].

The scalability of membrane contactors is generally linear because the available surface area is directly related to the ability to remove gases from a liquid of interest[3]. As noted with the carbonation of soft drinks, this principle can also be applied to the addition of gases to a liquid. Operational parameters will be optimized through experimentation. Membrane contactors have the distinct

advantage of a significantly higher contact area as a ratio of the space they take up, this is outlined in Table 4.1.

Table 4.1: Specific surface area of different phase contactors.[3]

Contactor	Specific surface area (m^2/m^3)
Free dispersion column	1-10
Packed column	100-800
Mechanically agitated column	50-150
Membrane contactor	1500-3000

To further illustrate the information in Table 4.1, a 10 inch diameter membrane contactor from Liqui-Cel® has a contact surface area of over $130m^4$. Given this information it is possible for membrane contactors to reduce the size of gas absorber or gas stripping units by up to 65%[3].

The Merril-Crowe process requires for a gold containing high pH cyanide solution be deaerated in order to facilitate efficient gold extraction. In the Merril-Crowe process zinc is added to this gold solution. If the dissolved oxygen content is not below 1.0ppm and ideally 0.5ppm the precipitation of gold from this cyanide solution is highly inefficient[5]. Current technology employs a large vacuum tower. The vacuum tower presents many issues such as worker safety, industrial footprint, and the difficulty in locating leaks in the vacuum system. A membrane contactor degassing system has the potential to not only be more

efficient but also much smaller than the conventional vacuum degassing tower. The membrane contactor system will likely be operated without a vacuum system instead using a nitrogen purge. This eliminates the difficulty in finding leaks on the vacuum system, ensuring that the unit operation is working at design efficiency.

4.3 Experimental:

The filtration system consisted of a steel base plate with aluminum scaffolding, with a pump located on the floor below the base. The tank is positioned directly above the pump on the steel base, as seen in Figure 4.2.

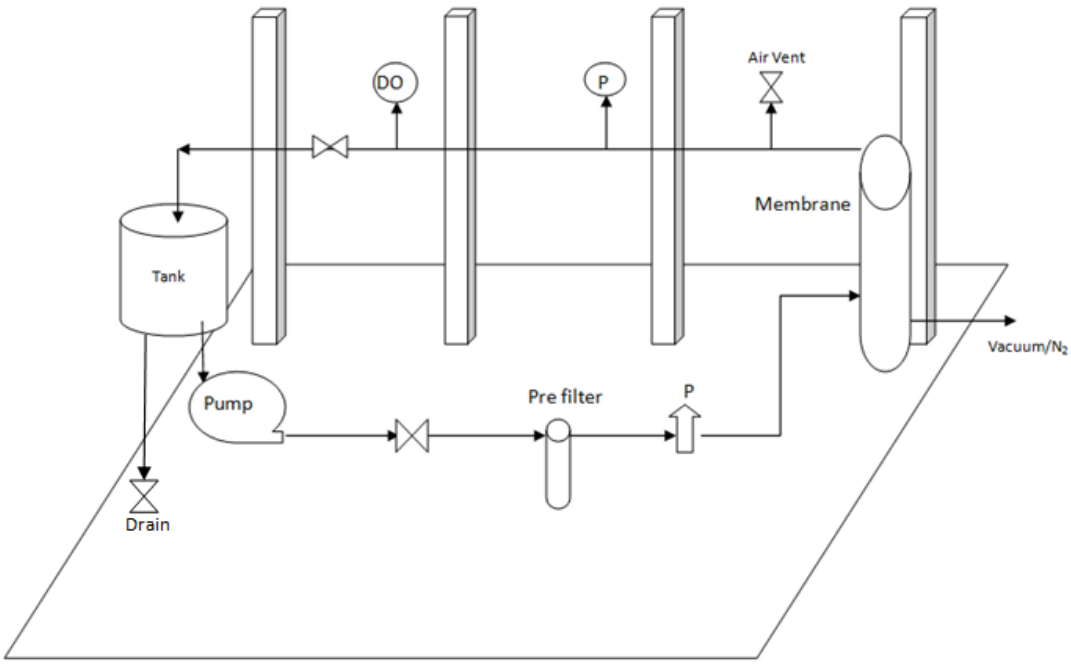

Figure 4.2: Schematic layout of filtration system on bench scale test skid.

Test solution, cyanide, or water flows through the pvc piping to the membrane where oxygen extraction occurs. Experiments were conducted with both a vacuum or nitrogen purge on the lumenside of the membrane. Nitrogen was purchased from AirGas and had a purity of 99.9% When a nitrogen purge was used as the driving force it was ran counter-current to the liquid flow to maximize efficiency. The dissolved oxygen concentration was measured with an inline meter, Eutech DO 500 with an accuracy of +2%. Considering a With valves at critical places on the system it was easy for the operator to control and test a variety of different system parameters. The Liqui-Cel® membrane, in which molecular oxygen extraction occurs was the 2.5x8 X40 membrane. Sodium cyanide was purchased from Sigma Aldrich and had a purity of 97%. The pH was raised by using anhydrous sodium hydroxide pellets also purchased from Sigma Aldrich with a purity of 97%. Each experiment was preset before with water so that upon starting the pump the system would reach the test conditions almost immediately. This was done to ensure that the results were not skewed because of the fast response time of the system to the driving force being applied across the membrane. Table 4.2 depicts the experiments conducted with the system. In each experiment the tank was filled with 3 gallons of solution at 25^0C equilibrate to atmospheric pressure in Reno, NV.

Table 4.2: Multi-factorial experiments performed on the bench scale membrane test stand.

Liquid Flow Rate(gpm)	Driving Force	Liquid Pressure (PSI)	Test Solution
1 and 3	-19.0 in Hg Vacuum	10 and 45	Distilled Water
1 and 3	N_2 2.4 SLPM	10 and 45	Distilled Water
1	N_2 7.0 SLPM	45	Distilled Water
1	N_2 7.0 SLPM	5,25,45	10.5pH+300ppm cyanide
1	N_2 7.0 SLPM	5,25,45	10.5pH

4.4 Results/Discussion:

Table 4.3 shows the final dissolved oxygen concentrations from the multifactorial experiments outlined in Table 4.2.

Table 4.3: Results of multifactorial design experiments.

System Pressure (PSI)	Gas Side Pressure (in Hg)	Flow Rate (gpm)	Final dissolved oxygen concentration (ppm)*
10	-19.0	1	0.79
10	-19.0	3	0.72
45	-19.0	1	0.6
45	-19.0	3	1.18
10	N_2 **	1	0.07
10	N_2**	3	0.02
45	N_2**	1	0.00 @ 7min&45sec
45	N_2**	3	0.00 @ 8min&54sec

* Concentration after 10 minutes unless otherwise noted, 0.00 defines undetectable dissolved oxygen

** The Nitrogen stream was counter current to the liquid stream with a flow rate of 2.4SLPM

As can be seen in Table 3 the experiments, which utilized a nitrogen stream to create the driving force of mass transfer across the membrane, were far more efficient than that of the vacuum. Further optimization was determined to be necessary, as even the best result required more than two passes of the entire tank volume to remove the dissolved oxygen to below a detectable level. The best results for each flow rate are shown as a function of time in Figures 4.3 and 4.4 below. The error bars denote the standard error encountered in the experiments. It is important to keep in mind that the 3gpm experiment reduced the dissolved oxygen concentration to undetectable levels in just less than 9 minutes that this would be the equivalent of running 9 filters of this size in series. In contrast the 1gpm experiment with a counter current nitrogen flow, as the driving force would only require 3 passes of the same size filter.

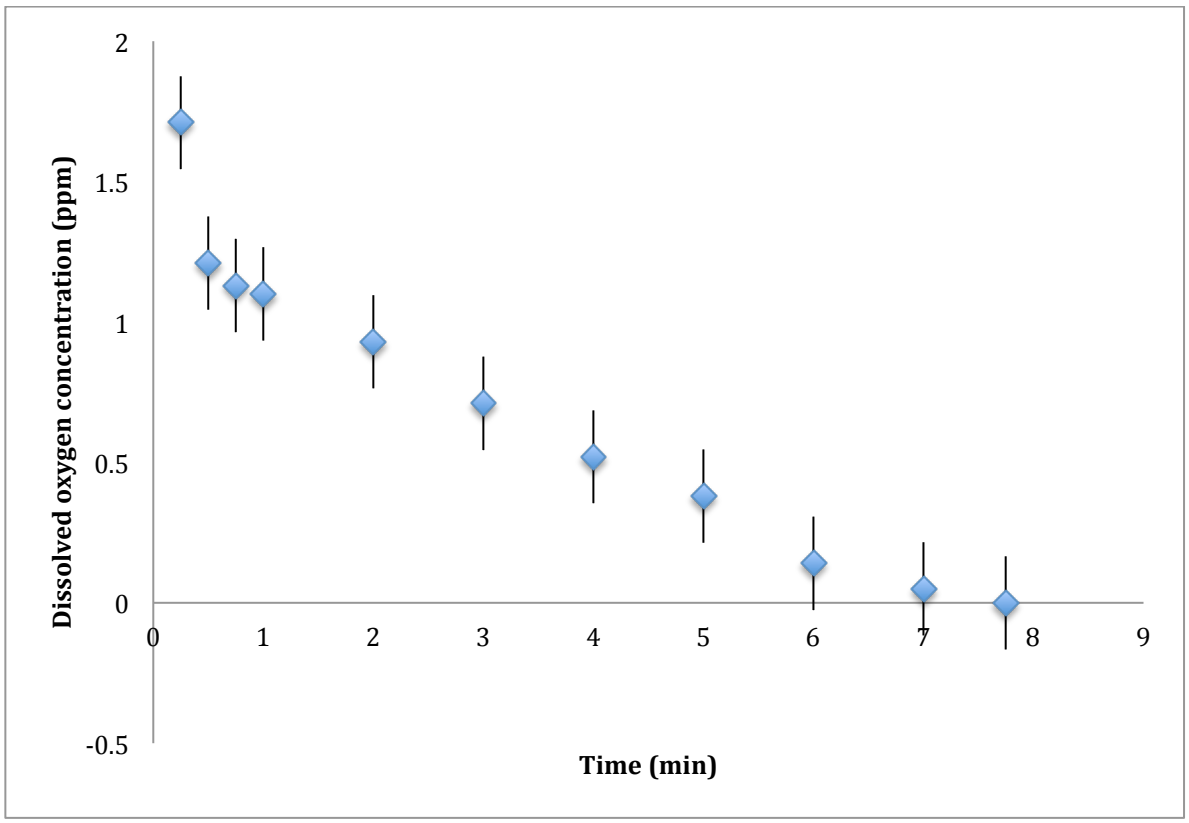

Figure 4.3: Dissolved oxygen concentration as a function of time for the following conditions: system pressure (10psi), liquid flow rate (1gpm), pressure drop (0.5psi), temperature (25.5C), nitrogen flow rate (2.4SLPM).

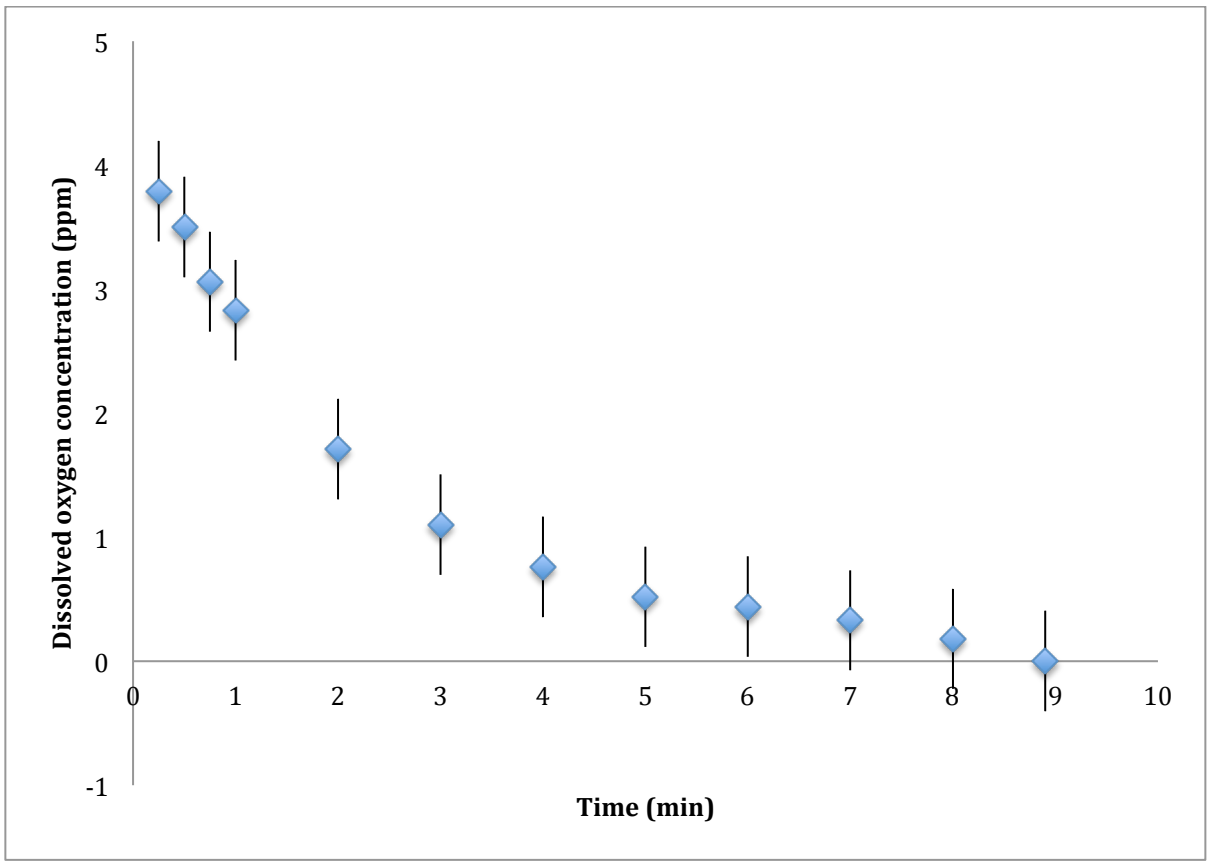

Figure 4.4: Dissolved oxygen concentration as a function of time for the following conditions: system pressure (45psi), liquid flow rate (3gpm), pressure drop (5psi), temperature (27C), nitrogen flow rate (2.4SLPM).

Over the course of the above experiments it was observed that at low flow rates of approximately 1gpm the pressure drop across the membrane was minimal at 0.5psi, the pressure drop at the higher flow rate of 3gpm was 5psi. These values corresponded with the expected pressure drop in the liquicel literature.

Further analysis of the effect of counter current nitrogen flow rate was done. Nitrogen flow rate was tested in three further experiments using only water. The change in purge gas flow rate did not have a discernable effect upon the rate of gas transfer out of the system. Table 4.3 shows the final results of each experiment. Each of the experiments in Table 4.3 was conducted until the trend of dissolved oxygen concentration stabilized. The stabilization occurred at ~90 seconds for each of the three different purge gas flow rates.

Table 4.4: Effect of purge gas flow rate upon the final dissolved oxygen concentration.

System Pressure (PSI)	Final dissolved oxygen concentration (ppm)	Purge Gas flow rate (SCFH)
45	0.12	10
45	0.14	20
45	0.15	30

The data displayed in Table 4.4 does show an upward trend as the purge gas flow rate is increased. This trend is exceedingly small and the margin of uncertainty for the sensor does not allow for the existence of the trend to be confirmed or denied. Given that a higher purge gas flow rate would lead to increased operating costs it is desirable to operate at the lowest possible flow

rate. While in actual operation the lowest purge gas flow rate would be chosen due to cost concerns, we chose the center flow rate to ensure robustness in the experiments. Choosing the center flow rate would theoretically allow a higher loading of dissolved oxygen without reducing the driving force.

The results of the experiments using the high pH and cyanide solution were consistent with previous work, however the final concentrations were not as low as with the pure water tests. Table 4.5 shows the final results for the cyanide and high pH solutions.

Table 4.5: Results of cyanide and basic solution experiments.

System Pressure (PSI)	Final dissolved oxygen concentration (ppm)	Solution
5	0.19	10.5pH + cyanide
25	0.71	10.5pH + cyanide
45	0.30	10.5pH + cyanide
5	0.13	10.5pH
25	0.38	10.5pH
45	0.14	10.5pH

The results shown in Table 4.5 demonstrate that the addition of cyanide and base to the solution being deaerated do not pose a problem with the efficiency of the membrane system. Each experiment followed the broad trend expected by Fick's[6] law of an exponential decay as seen in Figure 4.5.

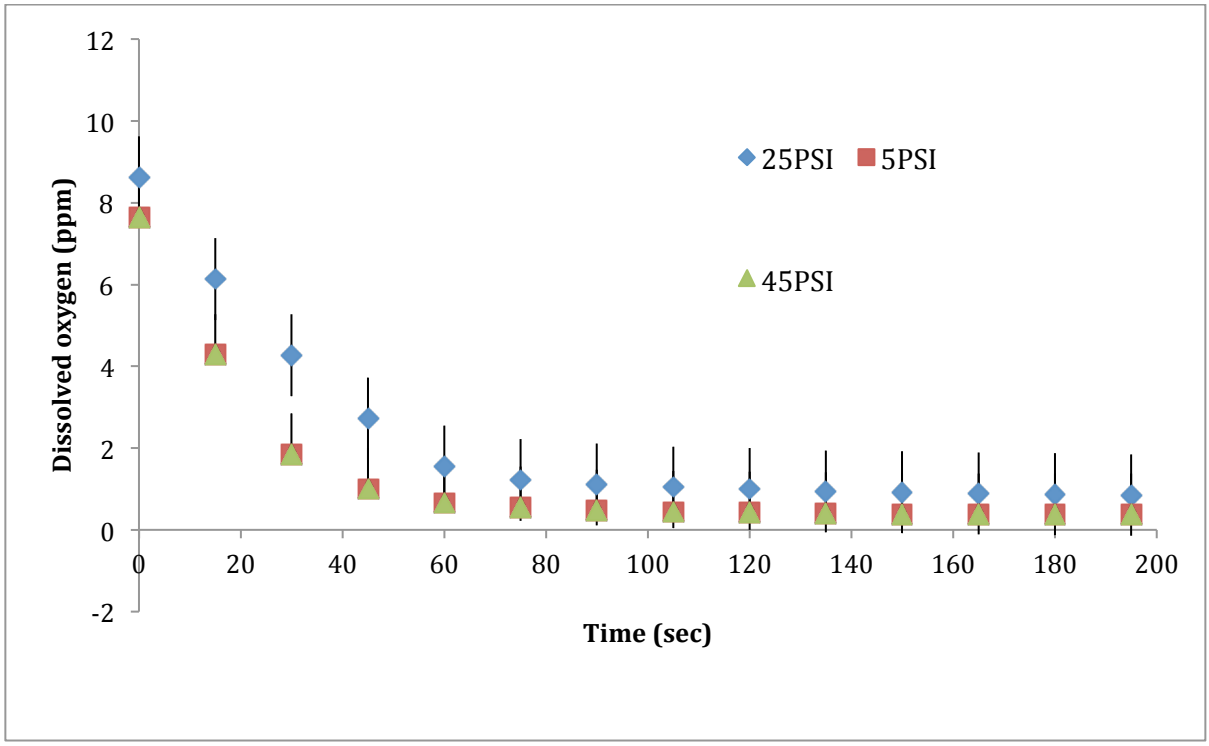

Figure 4.5: Dissolved oxygen concentration in a cyanide solution with a pH of 10.5.

The results shown in Figure 4.5 are very similar. The error bars denote an approximated amount of error at 1ppm of dissolved oxygen. This number was chosen because of the discrepancy in the starting values. The dissolved oxygen sensor was given a 2-point calibration before each experiment. This gives reason to believe the difference in starting values is due to sensor error. Prior to

each experiment the dissolved oxygen sensor was removed from the system and used to test the dissolved oxygen level present in the saturated solution about to be tested. interesting note is that the dissolved oxygen concentration never reaches an undetectable level as been shown to be possible in previous experiments. This is likely due to several factors, the holding tank being open and the operation of the dissolved oxygen sensor itself. Reaction 1 shows one of the reactions taking place at the electrodes of the sensor. In Reaction 1 the electrons present are from the oxidation of the silver anode. The silver anode is reduced by the electrolyte solution present in the sensor. This solution was changed every other experiment so as to ensure the presence of fresh electrolyte for the optimal operation of the dissolved oxygen sensor.

$$O_2+4e^-+2H_2O <=> 4OH^-$$

Reaction 1: reversible reaction taking place at the electrode[7].

When in a high pH environment we believe this reaction is being forced in the opposite direction if the dissolved oxygen concentration is low due to the large excess of hydroxide ions present. Table 4.5 supports this hypothesis because the final dissolved oxygen concentrations with and without cyanide in a high pH environment are very similar for equivalent experiments. Figure 4.5 shows that the exponential curve flatlines after 2 minutes where in previous experiments the curve continued to an undetectable level. The concentration to

time curve shown in Figure 4.5 is very similar to the curve observed without cyanide present.

The best results obtained from all experiments are shown in Figure 4.6, and Table 4.6 shows the system parameters.

Table 4.6: System parameters for the most efficient experiment.

System Parameter	Value
System pressure (psi)	45
Liquid flow rate (gpm)	1
Pressure drop (psi)	0.5
Counter current N_2 flow rate (SLPM,SCFH)	6.96,18
Temperature (Celsius)	26
System liquid volume (gallons)	3

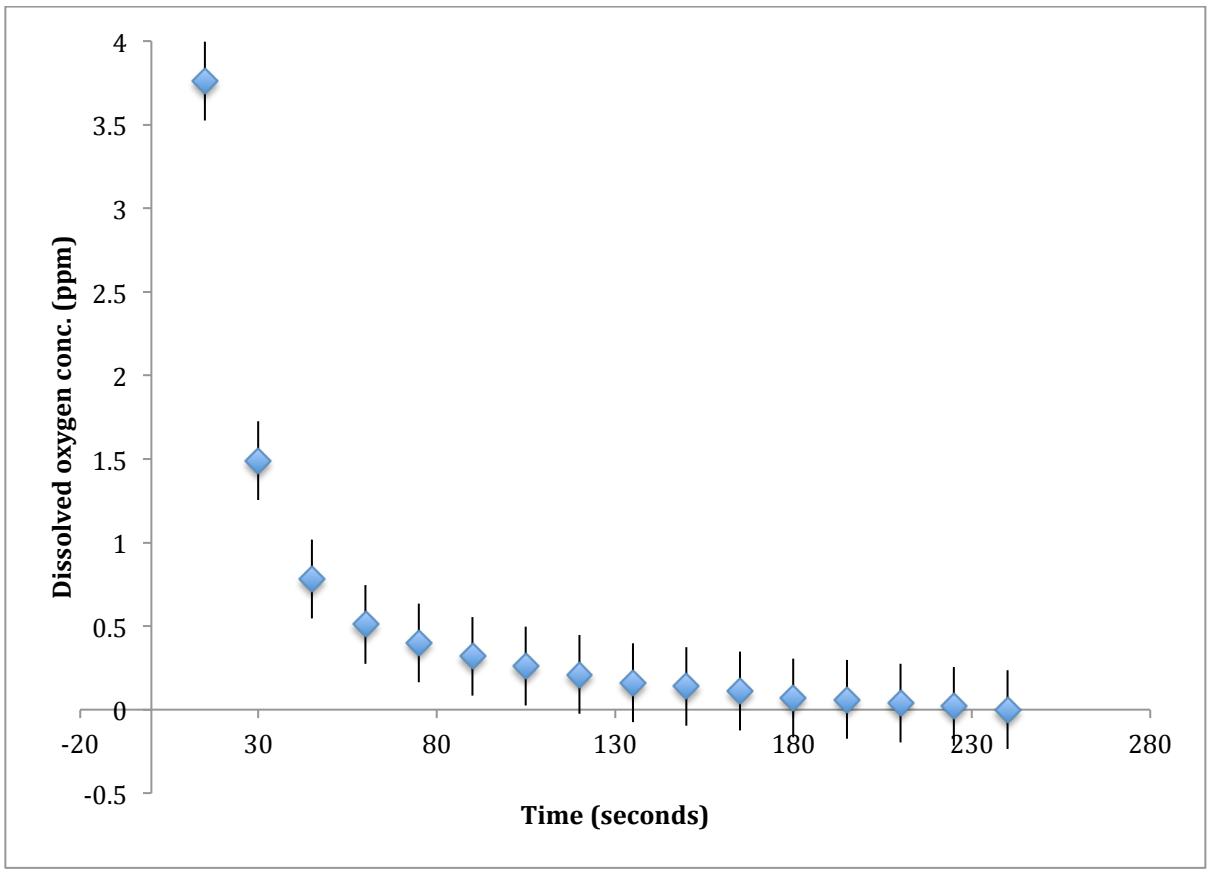

Figure 4.6: Dissolved oxygen concentration as a function of time for the system parameters in Table 3.

The results in Figure 4.6 show that the dissolved oxygen concentration became undetectable at 240 seconds of system runtime. This is equivalent to running the tank volume through the filter 1 pass and part of a second pass. With more optimization it appears to be possible to reduce the dissolved oxygen levels to an undetectable level in only 1 pass of the membrane contactor. With only modest pressure, and a low counter current nitrogen flow rate it appears as

though the membrane contactor facilitates the mass transport of dissolved oxygen out of the fluid with high efficiency.

4.5 Conclusions:

The results shown above demonstrate that the basic cyanide solution did not have an adverse effect upon the gas transfer possible with the membrane. A purge gas was determined to be necessary as the level of vacuum achievable on the system did not provide nearly the gas transfer that a purge gas was able to. Using a sensor that operates differently than the electrode currently used should demonstrate similar results whether the pH is elevated or not. The results are very promising for the intended application of deaeration in the Merrill-Crowe process. Several main points for the project are shown below:

- Membrane flux is $0.0588 gO_2/m^2 \cdot min$
- Final concentration of dissolved oxygen was between 0.13-0.71 with pH of 10.5 and/or cyanide present
- Purge gas flow rate had no discernible effect upon gas transfer as expected

Reducing the operational hazards, footprint and uncertainty as is present with the large vacuum towers typically employed for this unit operation could be a factor in adoption of this technology. We hypothesize that the combination of the benefits of the membrane system compared to current technology makes a

strong case for its implementation. While a grassroots system makes the most sense, a replacement of the vacuum tower might still be financially viable due to the safety and simple operation of a membrane contactor system.

4.6 Acknowledgements:

Dan Kappes and Dustin Albin at Kappes-Cassidy Associates are acknowledged for technical input and support for this project.

4.7 References:

[1] Wiesler F., Membrane Contactors: An Introduction to the Technology. Ultrapure Water *1996.*

[2] Mackey J, Mojonnier J. CO2 Injection using Membrane Technology. Bev-Plants '95 Eighth International conference, *March 1995.*

[3] A. Mansourizadeh, A.F. Ismail. Hollow fiber gas-liquid membrane contactors for acid gas capture: A review. J Haz Mat, *2009 38-53.*

[4] http://store.liqui-cel.com/DataSheet.aspx?ProductID=34 (Membrane contactor data sheet)

[5] Marsden, John, The Chemistry of Gold Extraction, Littleton, CO: Society for Mining, Metallurgy, and Exploration, 2006. Print.

[6] Webb, Stephen W., Karsten Pruess. *The Use of Fick's Law for Modeling Trace Gas Diffusion in Porous Media*. Transport in Porous Media: 327-341, 2003.

[7]Eutech DO 500 Manual

Chapter V: Economic Analysis and Design review of Membrane Contactor System

Process Description:

The clean process stream is sent into the membrane contactors. Depending upon system size several membranes will be operated in parallel. In a counter-current arrangement a purge gas of nitrogen will be sent through the lumen-side of the membrane. This will provide the driving force for the removal of oxygen. If the nitrogen is produced on site the waste nitrogen can be purified and reused indefinitely. The system will deaerate the process stream to an undetectable level of dissolved oxygen, approximately 0.01ppm. Figure 5.1 shows a basic process flow diagram of the proposed membrane contactor system and how it would fall into the broader Merrill-Crowe process.

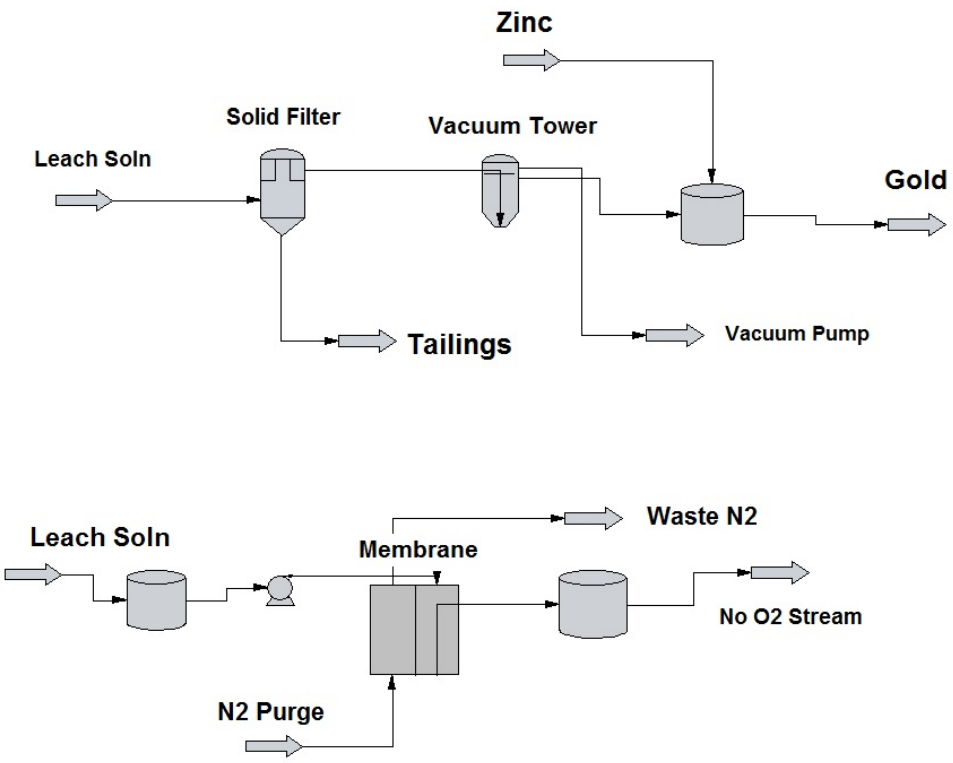

Figure 5.1: Process flow diagram of merrill-crow membrane contactor system.

Deaeration of gold cyanide solution before processing with zinc as done in the Merrill-Crowe process significantly increases the percent recovery of gold. The use of vacuum deaeration is common however the extent of oxygen removal can also have an effect upon the recovery of the gold in solution as well as the amount of zinc required for gold cementation. Several side reactions scavenge zinc from the system and make it unavailable for gold cementation, because of this a large excess of zinc must be used. Reaction scheme 2 below shows how one side reaction occurs[1]. If one was to take advantage of the efficient dissolved oxygen removal provided by membrane contactors we believe a significant

amount of zinc could be saved which would result in a large cost savings for the operation.

In order to give a reasonable estimation of what a membrane contactor system might cost, several projects have been chosen as case studies. The projects range in size from very large to small. The process volume for each system is then studied over several implementations. In the first instance a hybrid system where the current technology will do the bulk deoxygenation (target 0.5ppm DO), and the membrane contactors are used for the fine removal. These systems have an estimate for installation cost included in order to give a rough idea of the payback time for the capital cost.

The installation cost estimate is calculated using the equation below.

$$instal\square ation\ cost = 10{,}000 + 2{,}000(Number\ of\ membranes - 1)$$

The hybrid system estimates are based upon running each membrane at 600gpm.

Table 5.1: Projected cost of hybrid system for a process volume of 2514gpm.[1]

Number of Membranes	Projected cost ($)	Zn savings (ppm)	Annual Savings($)	Payback % per year
1	24000	1.5	15000	62.5
2	44400	3.0	30000	67.5
3	64600	4	40000	61.9

Table 5.2: Projected cost of hybrid system for a process volume of 4200gpm.[2]

Number of Membranes	Projected cost ($)	Zn savings (ppm)	Annual Savings($)	Payback % per year
2	44400	1.75	29400	66.2
3	64600	2.75	46200	71.5
4	84800	3.75	63000	74.5

Table 5.3: Projected cost of hybrid system for a process volume of 21500gpm.[3]

Number of Membranes	Projected cost ($)	Zn savings (ppm)	Annual Savings($)	Payback % per year
5	94200	1.00	85420	90.7
10	202000	1.75	149500	74.0
15	301000	2.75	234900	78.0

In Tables 5.4, and 5.5 we give base pricing for the membrane contactors only, this economic analysis does not take into account the operating costs of the membrane deaeration system. The membrane area required for the target dissolved oxygen concentration is based upon the experimental results acquired.

The two systems studied in Tables 5.4 and 5.5 are not hybrid systems and only use membrane contactors for deaeration of the process stream.

Table 5.4: Projected cost of several process volumes with a target dissolved oxygen concentration of <0.5ppm.

Process volume (gpm)	Membrane Area (m^2)	Projected cost ($)
2514[1]	2984	127400
4200[2]	4103	195800
21500[3]	20142	939600

Table 5.5: Projected cost of several process volumes with a target dissolved oxygen concentration of <0.01ppm.

Process volume (gpm)	Membrane Area (m^2)	Projected cost ($)	Projected savings ($)	Payback % per year
2514[1]	3917	178000	49670	27.9
4200[2]	5880	284800	83400	29.2
21500[3]	30100	1404000	427100	30.4

As can be seen from Table 5.4 and Table 5.5 the cost is significant but if the target dissolved oxygen concentration is raised the cost can be significantly reduced. While the higher end dissolved oxygen concentration is not ideal, the

system can be easily scaled to a lower target dissolved oxygen concentration or, a larger process volume. The high modularity and scalability of membrane contactors lends itself to this capacity.

Table 5.6: Projected cost savings of zinc per annum for test casses.

*Assuming $2000 per ton zinc powder[5]

Process volume (gpm)	Tons of zinc saved	Projected cost savings ($)
2514	24.8	49670
4200	41.7	83400
21500	213.5	427100

The cost savings in Table 5.6 do not take into account any benefit of increased rate or completeness of gold cementation due to the lower dissolved oxygen concentration in the pregnant cyanide solution. As demonstrated in Table 6 a small reduction in the amount of zinc scavenged by the pregnant cyanide solution greatly reduces the amount of zinc required for the efficient cementation of gold. Further cost savings could be realized if the pregnant solution contains more than the 300ppm sodium cyanide used for the calculations.

In another iteration of cost analysis the cost of pumps, tanks, and membrane contactors is considered. This analysis also follows a different

implementation procedure than the previously outlined systems. All of the following analysis is considering the 4500gpm system. The cost estimate from Table 5.7 was created using CAPCOST. The equipment specifications are shown below in Tables 5.8,5.9,5.10. The cost estimate from Table 5.7 is assuming that the system is being installed new and not replacing a current vacuum tower which would already have the necessary tanks and pumps. The cost is then reduced to $284,800, this gives a much more desirable payback period of 2.75 years.

Another option to replace a current vacuum tower system is to add several small modules each year (4 membrane contactors per year) in order to achieve a more favorable initial capital outlay. This approach is detailed in Table 5.11. The approach in Table 5.11 plays to two strengths of membrane contactors, which are the modularity of the system and the small footprint in comparison to a vacuum tower. Modularity of this approach would be similar to expanding an existing membrane contactor system to increase the process flow.

Table 5.7: Capital cost of the tanks, membrane contactors, and pumps identified for use.

Equipment	Number	Cost per unit ($)	Total Cost ($)
Tank	2	88,400	176,800
Pumps	2	28,400	56800
Membrane contactors	16	17,800	284,800
New Install Cost ($) = 518,400	Vacuum Tower Replacement Cost ($) = 284,800		

Table 5.8: Equipment specifications of pumps.

Material of Construction	Stainless Steel
Power (Shaft) kW	115
Efficiency	80%
Type/Drive	Centrifugal/Electric
Outlet Pressure	45psi

Table 5.9: Equipment specifications of tanks.

Material of Construction	Steel
Volume (gallons)	200,000
Type	Fixed Roof

Table 5.10: Equipment specifications of membrane contactors.

Housing Material of Construction	PVC
Membrane Material of Construction	Polypropylene
Membrane Area (m^2)	373
Purge Gas Flow Rate (SCFM)	6

Table 5.11 gives a running total of the expected zinc savings as well as the years to payback if the system was to incrementally replace the vacuum tower currently in use. The potential zinc savings on the 4500 gallon per minute study above is 107,443 dollars per annum.

Table 5.11: Cost of addition of 4 membrane contactor modules to replace a currently in use vacuum tower.

Module Number/ Installation year	Total Cost ($)	Total Zn Savings (ppm)	Total Savings($)	Annual Savings of system ($)	Years to Payback of complete system
1	73600	2.5	44760	44760	1.6
2	147200	3.5	107435	62675	1.4
3	220800	4.5	188015	80580	1.2
4	294400	6	295458	107443	1

The concentration of dissolved oxygen in the pregnant cyanide solution has a large impact on gold cementation[1]. One of the early struggles with the Merrill-Crowe process related to just that. With the introduction of the Crowe vacuum it became a much more economical way of processing a pregnant cyanide solution. Unfortunately the Crowe vacuum system only achieves a dissolved oxygen concentration of about 0.5ppm[4]. While this is quite low,

membrane contactor systems can easily achieve a dissolved oxygen concentration of less than 10ppb, based upon our experimentation. The advantages of stronger deaeration of the pregnant cyanide solution are demonstrated by Marsden Et Al.[4] The advantages being, stronger gold cementation as well as a higher zinc utilization, which can represent a significant cost savings as well as higher return on ore processing. Reaction Scheme 1 shows the heterogeneous reaction of the aqueous gold cyanide solution with solid zinc. As is clear it is imperative to keep the zinc in the solid phase and not allow it to be oxidized by the dissolved oxygen in the system as shown in Reaction Scheme 2. Figure 5.2 gives a graphical representation of the heterogeneous reaction taking place.

$$2Au(CN)_2^- + Zn + 4CN^- \leftrightarrow 2Au + 4CN^- + Zn(CN)^{2-}_4 \quad (1)$$

Reaction Scheme 1: Cementation of aqueous gold using solid zinc

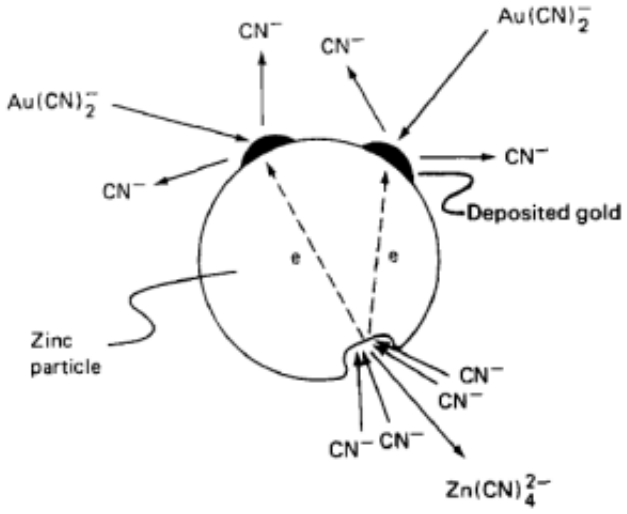

Figure 5.2: Mechanism of the precipitation of gold onto solid zinc.[4]

The solubility of zinc increases with increasing dissolved oxygen concentration; this is compounded by higher cyanide concentrations. Figure 5.3 shows this effect with several different cyanide concentrations.

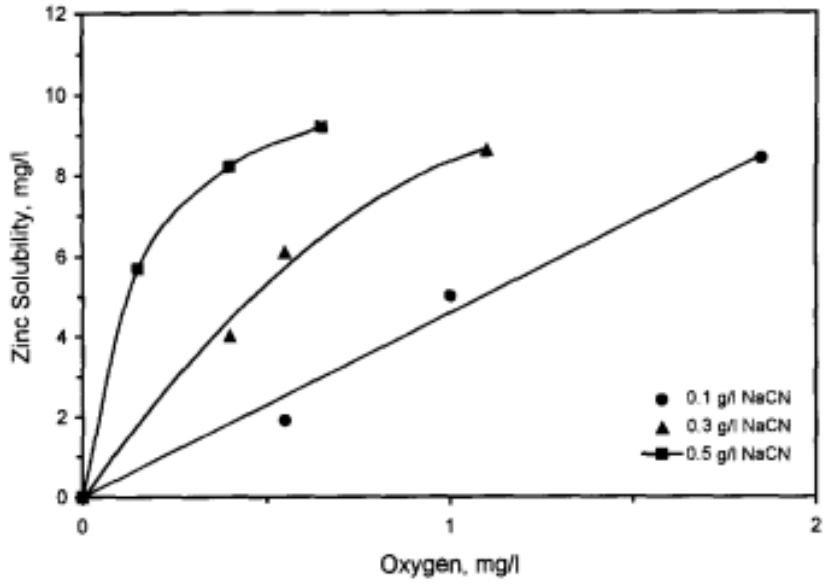

Figure 5.3: Zinc solubility as a function of dissolved oxygen concentration and sodium cyanide concentration.[4]

As can be clearly seen as the concentration of dissolved oxygen increases the solubility of zinc also increases. This is demonstrated by reaction scheme 2, where oxygen plays a crucial part in the complexing of elemental zinc with cyanide.

$$2Zn + O_2 + 8CN^- + 2H_2O \leftrightarrow 2Zn(CN)_4^{2-} + 4OH^- \qquad (2)$$

Reaction Scheme 2: side reaction of zinc, oxygen, cyanide

The above reaction and other side reactions with zinc can consume from five to thirty times the required stoichiometric amount for the gold cementation

reaction[11]. By lowering the dissolved oxygen content to well less than 0.5 ppm the amount of zinc scavenged can be drastically reduced. This can lead to a significant operating cost reduction over time. Considering a 0.3g/l NaCN (300ppm) concentration with 0.5ppm of dissolved oxygen present the solubility of zinc is approximately 6mg/l. Reducing the dissolved oxygen content to ~10ppb would lower the solubility of zinc to approximately 1mg/l. Table 5.6 shows the projected cost savings a membrane contactor system could provide per annum simply by reducing the amount of zinc required for gold cementation.

References:

[1] Bear Creek Mining, Santa Ana project feasibility study

[2] Coeur Rochester, Inc: Plant-Wide energy consumption, Rochester Nevada

[3] Allied Nevada Gold: Hycroft gold mine

[4] Chi, Gexla, Maurice C. Fuerstenau, and John O. Marsden. "Study of Merrill-Crowe Processing. Part I: Solubility of Zinc in Alkaline Cyanide Solution." International Journal of Mineral

Processing 49.3 (1997): 171-83.

[5] www.alibaba.com zinc powder bulk estimate

Chapter VI: Future Work

Sulfur diffusion through polyurethane:

After the development of a worst case scenario from the experiments done in Chapter 2, it would be of interest to do a more realistic set of experiments at atmospheric temperature and concentration of sulfur that would potentially be encountered in different environments. This would enable the development of a more robust model to so that a more complete picture of the phenomena could be developed. To verify the assumption that the reaction time could be neglected another set of experiments could be conducted using nanoparticle silver instead of the relatively large particles used in Chapter 2. The change in the speed of reaction would ensure that the reaction time was significantly faster than the diffusion timescale.

Polyphenylquinoxaline as a sacrificial heat exchanger coating:

The thermal conductivity of PPQx was well established. Future efforts should focus on enhancing the thermal properties so as to make the coating more desirable for use in a heat exchanger. Preliminary work was done in this direction with the silicone carbide and tungsten powders. Abrasion testing should also be performed so as to determine the durability of the polymer coating in an abrasive environment. Silicone carbide and tungsten should also help increase the abrasion resistance of the polymer. Other methods of coating

beyond the physical application would potentially be beneficial to explore. The difficulty in coating the interior of pipes could present problems and different coating methods could proactively eliminate this concern.

Deaeration of a basic cyanide solution:

To make future experiments more successful several changes need to be made to the bench-scale system. The tank should be fully enclosed to more closely simulate an industrial unit operation. Placement and type of dissolved oxygen sensor needs to be reevaluated, as it appears to have caused more error to be introduced into the results than would be desirable. Testing of the membrane on an actual process stream over a long time frame would be highly insightful, as it would help determine if any scaling, or fouling issues arise. By testing the system on an ever-changing process stream any issues resulting from chemistry changes could be identified.

The system is designed and proposed to be more efficient in terms of zinc consumption. To prove this theory extensive experimentation to determine if the gold continues to precipitate with lower levels of added zinc. The results of these experiments will prove or disprove the viability of the system as a replacement of a vacuum tower currently in use. If the extra financial benefit is not present it would likely be preferred to utilize the method in a grass-roots installation rather than as a replacement system.